SOFTWARE FOCUS

WIREs COMPUTATIONAL MOLECULAR SCIENCE WILEY

Growing Spicy ONIOMs: Extending and generalizing concepts of ONIOM and many body expansions

Phillip Seeber [ORCID] | Sebastian Seidenath [ORCID] | Johannes Steinmetzer [ORCID] |
Stefanie Gräfe [ORCID]

Institute of Physical Chemistry, Friedrich
Schiller University Jena, Jena, Germany

Correspondence
Phillip Seeber, Institute of Physical
Chemistry, Friedrich Schiller University
Jena, Helmholtzweg 4, 07743 Jena,
Germany.
Email: phillip.seeber@uni-jena.de

Edited by: Peter Schreiner, Editor-in-Chief

Abstract

The ONIOM method and many extensions to it provide capabilities to treat challenging multiscale problems in catalysis and material science. Our open-source program *Spicy* is a flexible toolkit for ONIOM and fragment methods. *Spicy* includes a generalization of multicenter-ONIOM, a higher-order multipole embedding scheme, and fragment methods as useful extensions of our own *n*-layered integrated molecular orbital and molecular mechanics (ONIOM), which allow applying ONIOM and high accuracy calculations to a wider range of systems. A calculation on the metallo-protein hemoglobin demonstrates the versatility of the implementation.

This article is categorized under:

    Electronic Structure Theory > Combined QM/MM Methods

    Molecular and Statistical Mechanics > Molecular Interactions

    Quantum Computing > Theory Development

KEYWORDS

fragment methods, multiscale methods, quantum chemistry, software

1 | INTRODUCTION

Computational chemistry has long been restricted to molecules of only a few atoms. Drastic improvements both in the capabilities of computer hardware and the theoretical models themselves provided access to larger and more complex chemical systems and methods with ever-increasing accuracy.[1] Nowadays, many chemical problems are related to interactions and behaviors of, among others, biomolecular systems, soft matter, or complex catalysts, necessitating reliable and efficient computational models. Many of those problems inherently possess multiscale character, as spatially small effects in large systems are to be investigated, that is, catalytic reactions of small molecules in the active center of large enzymes,[2,3] interactions of small substrates with large zeolites,[4] or dye–polymer interactions.[5]

The development of the fundamental theoretical models continues, and with linear scaling self-consistent field (SCF),[6–11] correlation,[12–19] and density matrix embedding methods,[20,21] the quantum mechanically accessible system size grew tremendously. Force fields now allow to simulate entire viruses[22] and interface reactions up to the millimeter scale.[23] A different idea is employed by the quantum mechanics/molecular mechanics (QM/MM)[24–27] and ONIOM[28–30] multiscale approaches that aim to combine advantages of different methods to provide a tailorable system partitioning

and description. Large but well-behaved parts of the chemical system can be described with low-cost methods, such as force fields, while smaller regions, where quantum effects play an essential role, or high accuracy is required, can be described with more precise but also computationally more demanding quantum mechanical methods. Thus, QM/MM and ONIOM have been successfully employed to describe the photophysics of proteins and deoxyribonucleic acid (DNA),[31–34] processes in soft matter materials,[35] catalytic processes,[36–38] inorganic materials,[39–41] reactive chemistry,[42] and more. In recent years, many implementations for QM/MM and ONIOM methods have emerged or have been improved; LiCHEM[43] and QM/MM[44] implement polarizable QM/MM methods, which can improve the description of ground and excited states. PyChemShell,[45] ASE,[46] and Cuby[47] implement QM/MM with electrostatic embedding, as parts of a larger computational chemistry frameworks, with access to a multitude of interfaced programs. ORCA[48,49] has recently implemented a set of QM/MM and ONIOM methods with electronic embedding.[50,51] The MRCC program package[52] in its latest version supports ONIOM with an arbitrary number of layers and inclusion of solvent effects via the polarizable conductor model (PCM).[53] Gaussian[54] offers a mature ONIOM3 implementation with micro-cycle driven optimizations and electronic embedding.

Despite the success of existing QM/MM and ONIOM methods, there remain classes of chemical systems, that push these methods to their limits. We are interested in describing interactions in electronically active soft matter materials, often in conjunction with embedded (photo)catalysts. For example, the integration of (photo)catalysts or photosensitizers into tailored polymer membranes can synergistically improve the stability of the active species and kinetic aspects while simplifying the handling of compounds sensitive to oxygen exposure.[55,56] An accurate description of their electronic properties and rich photochemistry prohibits their sole treatment by molecular mechanics (MM) methods. At the same time, a naive separation into low- and high-level regions may be impossible, as important electronic effects may occur in the entire polymer. Another popular example for delocalized, cooperative effects is hemoglobin, which exhibits large-scale structural changes when oxygen binds to the four heme centers.[57,58] All hemes are equally important, and association/dissociation of oxygen in one heme involves structural changes in the entire protein. Studying all heme centers simultaneously in a QM/MM or ONIOM setup using accurate, quantum mechanical approaches is, however, computationally very demanding.

To this date, many modifications of the original ONIOM method have been proposed. Multicenter (MC)-ONIOM allows independent calculation of multiple, non-coupling sites in a macromolecular system.[59] Generalized-ONIOM combines the many body expansion (MBE) fragment method with ONIOM in an attempt to describe large layers with quantum mechanical methods.[60] In combination with the generalized many body expansion (GMBE) and fragment combination ranges (FCR), even more flexible system partitions become possible, while at the same time also providing a different approach to multiscale/multilayer methods.[61,62] Fragment methods allow splitting the full system into many smaller calculations, and the fragment size can be adapted to accurately describe encountered electronic effects, for example, in conductive polymers. In contrast to ONIOM, fragment methods do not imply a hierarchical order. The X-Pol method provides a formalism for polarizable electronic embedding, even in these more complicated setups.[63] ONIOM-XS allows to adapt the system partitioning as needed by dynamic reassignment of fragments to different layers during molecular dynamics (MD) or geometry optimizations.[64] Such an approach is especially useful for handling large structural changes, for example, following an electronic excitation or associative/dissociative processes in enzymatic reactions. The quality of electronic-embedding ONIOM strongly depends on the employed embedding charges. A powerful and flexible method to derive distributed higher-order multipoles is the distributed multipole analysis (DMA).[43,65–67] Together with fragment methods, DMA can provide accurate electronic multipoles for embedding at the quantum mechanics (QM) level of theory. In combination, versatile and flexible simulation setups in the extended ONIOM formalism can be realized. However, these methods are not widely applied, as integrated implementations are not commonly available.

In this article, we present the *Spicy* program, a well-integrated and user-friendly driver to carry out large-scale ONIOM calculations, with support for flexible fragment selection, and generation of high-quality embedding charges by means of DMA. Care was taken to implement these methods in a generic way, without restricting *Spicy* to a certain class of systems, for example, proteins. *Spicy* follows the approach taken by ASE,[46] pysisyphus,[68] LiCHEM,[43] and wraps computational chemistry programs to gain access to a wide range of computational models, which allows combining methods, that are not available within a single suite. Section 2 starts with a brief introduction to ONIOM, followed by a generalization of MC-ONIOM to arbitrarily nested multicenters. Electronic embedding and generation of higher-order multipoles is discussed in Section 2.2. Sections 2.3 and 2.4 provide details on how fragment methods are combined with our MC-ONIOM implementation and how micro-cycle driven optimizations are carried out. We will also discuss details of the implementation and how *Spicy* is developed in Section 3. Finally, illustrative test calculations will be presented

in Section 4. With *Spicy*, we provide a useful, modern open-source implementation written with a high level of abstraction that will serve as a foundation for further developments, and complement the advances of multiscale methods in recent years.

2 | THEORY

Originally, ONIOM emerged as a generalization of the integrated molecular orbital + molecular orbital (IMOMO)[28] and integrated molecular orbital + molecular mechanics (IMOMM)[69] schemes, which allow using different levels of theory for different parts of a chemical system.[28] Given a set of atoms A comprising the real (full) system, a proper subset $A_m \subset A$ is chosen, which defines the so-called model system, a region usually treated with a more accurate and expensive level of theory. This system separation may lead to dangling bonds in the model system if a bond between any atom $a \in A_r$, $A_r = A \smallsetminus A_m$, and any atom $b \in A_m$, existed. Sophisticated approaches to treat those boundaries between the regions have been proposed, for example, tailored effective core potentials (ECPs),[70–72] or freezing localized molecular orbitals.[73–75] The simplest approach is the introduction of link atoms, commonly hydrogen atoms, to saturate the open valence.[76,77] By positioning the link atom at r_{ab}^l along the vector of the cut bond $r_a - r_b$, no additional degrees of freedom are introduced.

$$r_{ab}^l = r_b + g_{ab}(r_a - r_b). \tag{1}$$

A reasonable value for the factor g can be obtained as a ratio of the covalent radii R^{cov} of the involved atoms

$$g_{ab} = \frac{R_b^{cov} + R_l^{cov}}{R_a^{cov} + R_b^{cov}}, \tag{2}$$

but empirically tuned values for g were also proposed.[78] The link atom approach has several advantages; it does not require implementation of a special Hamiltonian or orbital optimization procedure, works for any combination of MM and QM methods, and does not require tuned or system-specific parameters, for example, capping ECPs. Therefore, it is also applicable in setups, where, for example, an orbital localization scheme is not implemented, or a MM layer needs to be embedded.

Contrary to additive QM/MM (Equation (3)), the ONIOM energy is obtained from a subtractive scheme. While often formulated for two layers (ONIOM2, Equation (4)), the subtractive scheme easily generalizes into an arbitrary number of layers (ONIOM*n*).[28] Both IMOMM and IMOMO can be rewritten as a two-layered ONIOM expression (Equation (4)), and the combination of both (one outer layer molecular mechanics, and two layers quantum mechanics) can be written as a three-layered ONIOM-expression (Equation (5)).[28]

$$E_{QM/MM} = E_{QM} + E_{MM} + E_{QM\text{-}MM}, \tag{3}$$

$$E_{ONIOM2} = E_{r,c_1} + E_{m,c_2} - E_{m,c_1}, \tag{4}$$

$$E_{ONIOM3} = E_{r,c_1} + E_{i,c_2} - E_{i,c_1} + E_{m,c_3} - E_{m,c_2}. \tag{5}$$

Here, the subscripts r, i, and m refer to the real, intermediate, and model systems, and the c_j refer to calculation levels, which typically become more accurate with increasing j. ONIOM is considered an extrapolation scheme for the energy of the real, large system at a high calculation level. It has been noticed early, that the scheme generalizes to an arbitrary amount of layers n, which is then called ONIOM*n*.[28] In analogy to the system's energy, other extensive properties P can be calculated by the same scheme. The nuclear derivatives of the energy, the gradient g, and Hessian H are not extensive properties but become extensive when projected into the basis of the parent system before applying the ONIOM extrapolation.[78] This projection is given as

$$\overline{\mathbf{g}}_i = \mathbf{g}_j \mathbf{J}_j \tag{6}$$

$$\overline{\mathbf{H}}_i = \mathbf{J}_j^T \mathbf{H}_j \mathbf{J}_j, \tag{7}$$

where the properties from a layer j are projected into the basis of its parent system i, $\mathbf{J}$ denotes the Jacobian, and $\overline{\mathbf{g}}_i$ and $\overline{\mathbf{H}}_i$ are the nuclear derivatives of layer j expressed in the basis of i. The link atoms introduced in the model system are not present in the real system. Thus, their contributions to the nuclear derivatives are redistributed to their respective partners a and b in the real and model system, so that no additional degrees of freedom are introduced. Therefore, the Jacobian projects from the link-atom-augmented model system $A'_m = A_m \cup A_{m,l}$, where $A_{m,l}$ is the set of link atoms of the model system, to the real system with the atoms A. For a system with $m = |A'_m|$ atoms in the augmented model system and $n = |A|$ atoms in the real system, the Jacobian is of the form $3m \times 3n$ and is written as

$$\mathbf{J} = \begin{pmatrix} \mathbf{J}_{11} & \cdots & \mathbf{J}_{1n} \\ \vdots & \ddots & \vdots \\ \mathbf{J}_{m1} & \cdots & \mathbf{J}_{mn} \end{pmatrix} \tag{8}$$

$$\mathbf{J}_{ba} = \mathbf{E} \cdot \begin{cases} g_{o_a} & o_a \in A_{m,l} \wedge p_b \text{ is the real host partner of } o_a \\ 1 - g_{o_a} & o_a \in A_{m,l} \wedge p_b \text{ is the model partner of } o_a \\ 1 & o_a = p_b \\ 0 & \text{otherwise,} \end{cases}$$

where $o_a \in (A'_m = \{o_1, \ldots, o_m\})$ and g_{o_a} is a link factor calculated by equation 2 is o_a is a link atom, $p_b \in (A = \{p_1, \ldots, p_n\})$, and $\mathbf{E}$ is the 3×3 identity matrix.

So far, inter-layer interactions are only treated in the real system at the low level of theory and the mechanical coupling introduced via link atoms. However, the atoms of the set A_r are not visible to the atoms of A_m, and important interactions, that is, electrostatic attractions and repulsions, hydrogen bonds, or polarization effects in the model system, are entirely ignored. A substantial amount of such interactions can be captured by electronic embedding schemes.[29] In such schemes, point charges assigned to each atom in set A_r are used to embed the model system, mimicking the electric field of the environment. The costs of this approximation are twofold. First the costs to obtain a point charge model of the real system, and second those to account for the electric field in the calculation of the model system. The latter is possible in most quantum chemistry codes, as embedding charges are easily considered via an additional term in the one-electron operator in the Hamiltonian of a QM calculation

$$\widehat{H}_m^{\text{pol}} = \widehat{H}_m - \sum_{e,N} \frac{q_N}{r_{eN}} + \sum_{J,N} \frac{Z_J q_N}{r_{JN}}. \tag{9}$$

Here, in the Hamiltonian for the model system $\widehat{H}_m$, e refers to the electrons of A'_m, J to the nuclei of A'_m, and N to the point charges of A_r. Point charges q_N can be determined by various methods. While charge models such as Mulliken,[79] Löwdin,[80] or MM-charges come nearly for free, others, for example, restricted electrostatic potential (RESP)-charges,[81] may be costlier than the wavefunction calculation itself. While electronic embedding often significantly improves the accuracy of the ONIOM extrapolation, it also comes with a few pitfalls: (i) Nucleus-centered point charges are not observables, and the charge model cannot be uniquely defined. Charges obtained from commonly employed models can vary widely, for example, between Mulliken-,[79] Löwdin-,[80] and RESP-charges.[81] (ii) Short distances between atoms of A'_m and A_r can result in overpolarization of model system atoms close to the border. This is especially problematic when a link atom between a pair of atoms $a \in A_r$ and $b \in A_m$ is present, as this link atom is closer to the point charge representation of atom a than chemically reasonable. Such problems are usually avoided by scaling or deleting point charges in A_r, that are within a given distance (real space or in terms of bonds) to an atom in A_m.[29] (iii) Positive partial charges close to atoms of A'_m attract electrons. This can lead to unphysical electron density localization around those positive partial charges, as the atom of A_r, that is replaced by a simple point charge would also have repulsive effects on

electrons via Pauli repulsion.[82] (iv) The sum of the point charges of A_r is usually a non-integer number. Only A and A'_m are required to sum up to the respective system's charge. Nuclear gradients of the model system depend on the gradient of the embedding charges of the real system with respect to the nuclear coordinates. In principle, this derivative coupling requires derivatives of the embedding charges, which is only possible for a limited set of point charge models, for example, Löwdin charges.[83]

In Sections 2.1 and 2.2, we will describe how *Spicy* generalizes the classical ONIOM extrapolation scheme by allowing more flexible system setups and how the accuracy and robustness of electronic embedding are improved. We will also describe how fragment methods are used to approximately describe ONIOM layers in Section 2.3, and how the micro-cycle driven optimization scheme is generalized to arbitrary ONIOM setups in Section 2.4.

2.1 | Arbitrary multicenter ONIOM

So far, ONIOMn has been defined as an extrapolation scheme with a strictly linear layout of calculation layers, that is, there is exactly one model layer embedded in its parent layer. In 2003, Hopkins and Tschumper proposed an ONIOM2 scheme that allows defining multiple, non-overlapping models.[59] Later it was also extended to overlapping model systems.[84] The intersection corrections, that appear in those terms resemble those of the GMBE,[61] which is discussed in Section 2.3. However, there is no reason to permit only two layers (see Figure 1).

An arbitrarily deep ONIOMn scheme, where each system can have any number of non-overlapping subsystems, is conveniently represented as a rooted tree; see Figure 1 for an example layout with four layers, and eight (sub)systems. We will refer to such MC-ONIOM layouts with n layers as MC-ONIOMn. Each (sub)system in a MC-ONIOMn tree is identified not only by its depth in the tree, but more specifically by a sequence of steps $(i_k)_{k=0}^{n-1}$ relative to the root, which is called a path. The length of the sequence $d_{(i)} = |(i)|$ determines the depth in the tree. In the following, we will use this path equivalent to the respective node and its properties. Therefore, $\max_{(i) \in O} |(i)| = n-1$ in the MC-ONIOMn terminology, where O is the set of all node-identifying sequences of the MC-ONIOMn tree. For example, the node "BA" in Figure 1b can be reached by the sequence (B, A) starting from the root, and is at depth $d_{(B, A)} = 2$. We can now denote a set of children $C_{(i)}$ for each node (i),

$$C_{(i)} = \{(j) \in O \,|\, (i) \subset (j) \wedge |(i)| + 1 = |(j)|\}, \tag{10}$$

which is the set of index sequences leading to the children of (i). We can also define a set of nodes D_d at the same depth d in the tree

$$D_d = \{(i) \in O \,|\, |(i)| = d\}. \tag{11}$$
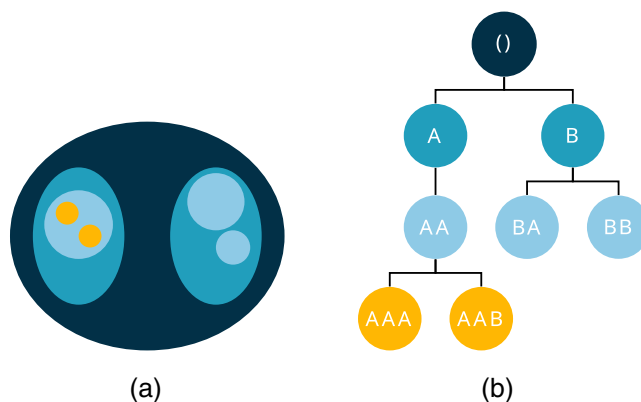
FIGURE 1   Representations of a MC-ONIOM layout with four levels and multiple subsystems in the first three levels. The rooted tree representation of a standard ONIOM3 setup would be a linear tree of three nodes without branching. In 0 colors represent the depth of subsystems in the ONIOM setup, while the disjoint ellipsoids of same color represent disjoint model systems in an embedding parent layer. In an equivalent representation in 0, each node represents a (sub)system in ONIOM, starting with the real layer 0 as the root of the tree. Colors represent the depth of a subsystem in the tree.

Given the example in Figure 1, the set of nodes at depth $d = 2$ is $D_2 = \{(A, A), (B, A), (B, B)\}$.

Employing this nomenclature, the notion of "non-overlapping subsystems" as stated earlier, can be formalized: Given any node (i) with its set of atoms $A'_{(i)}$, of which some may be link atoms, the subsystems of (i) form a disjunct family of sets of atoms over $A'_{(i)}$ denoted $A_{C_{(i)}}$, thus

$$A_{(j)} \cap A_{(k)} = \emptyset, (j) \neq (k) \wedge (j), (k) \in C_{(i)}$$
$$\bigcup A_{C_{(i)}} \subset A'_{(i)} \tag{12}$$

Each subset in the family of sets over $A'_{(i)}$ may then be augmented as necessary with link atoms. The notion implies that link atoms $A_{(i),1}$ of $A'_{(i)}$ become real atoms in $A_{C_{(i)}}$ if included in any of the subsystems. Thus, the link atom property is not inherited from one node to another.

The two calculations for each node (one for the root) are performed by walking the tree in depth-first order. A second depth-first walk is used to calculate extensive properties P in the spirit of the original ONIOM extrapolation scheme. For this purpose, every node (i) and its children $C_{(i)}$ can be understood as a MC-ONIOM2 setup. Starting from the base case, the terminal nodes of the tree, whose properties are not subject to extrapolation, all terms can be collected in a recursion of MC-ONIOM2 layouts

$$P_{(i)} = P_{(i)}^{c_{(i)}} + \sum_{(k) \in C_{(i)}} \left(P_{(k)} - P_{(k)}^{c_{(i)}} \right), \tag{13}$$

where in analogy to Equations (4) and (5), $c_{(i)}$ denotes the level of theory originally defined for node (i). If (i) has no children $(C_{(i)} = \emptyset)$, the recursion terminates. Equation (13) is therefore a depth first walk through the tree and $P_{()}$ is the desired target property, where $()$ denotes the root of the tree. Again, the nuclear gradient and Hessian have to be projected into their parent system's basis to become extensive properties (see Equations (6) and (7)).

2.2 | Electronic embedding

As noted earlier, the original mechanical embedding used in ONIOM and QM/MM misses the interlayer electrostatic interactions. In principle, intermolecular electrostatic interactions can be well described by a multipole expansion of their electric fields. However, the convergence radius of such multipole expansions is usually impractically large and requires the interaction spheres of the involved molecules to be well separated.[67] Unfortunately, well separated interaction spheres are nearly never encountered in typical ONIOM and QM/MM setups. Instead, often the opposite is observed: one of the molecular systems will be surrounded by the other, for example, the active center of an enzyme within a pocket of the protein backbone. For IMOMM setups, where partial-charge providing force fields are involved, the atom-centered partial charges of the MM part can be included in the one-electron operator of the QM calculation to account for this embedding effect (Equation (9)).[29] IMOMO-like ONIOM setups, with one QM layer embedding another one, are also possible, and the embedding partial charges of the real system are commonly obtained by a partial charge analysis.[83,85,86] This representation by point charges can be viewed as a distributed monopole expansion of the molecular electric field, dramatically reducing the convergence radii of multipole interactions and thus allowing to adequately treat the difficult situation of embedded molecules. In *Spicy* we employ a robust higher order expansion of the electric field as obtained by Stone's DMA, or its grid-based version GDMA.[65,66] DMA relies on the fact, that a multipole moment of order $l_a + l_b$ originates at the overlap centers of two basis functions of angular momenta l_a and l_b. The method also supports relocating these multipole moments to arbitrary expansion centers, for example, the atomic nuclei. A distributed expansion of the electric field up to quadrupoles has been shown to be in excellent agreement with the true electrostatic potential.[67] Unfortunately, most computational chemistry programs cannot incorporate higher-order multipole terms into their Hamiltonians and are limited to distributed point charges. Such restrictions are circumvented by approximating a higher-order DMA multipole expansion only through point charges. This way, the good agreement of the multipole expansion with the true embedding potential is maintained while the resulting monopoles can be taken into account in most quantum chemistry codes. Gao et al.,[87] and shortly after that Devereux et al.,[88] have

employed arrangements of point charges, called the distributed charge model (DCM), to represent a multipole expansion up to the quadrupoles. The method is also employed by the QM/MM program LiCHEM, which allows performing polarizable QM/MM calculations with the AMOEBA force fields and incorporates AMOEBA's higher-order multipole moments in the QM calculation.[43,89]

We will briefly recapitulate on the distributed multipole model, its conversion to a DCM, discuss possible edge cases, and how it applies to arbitrary MC-ONIOMn. An arrangement of six-point charges can represent a multipole expansion up to second order (quadrupoles) if the point charge coordinates are chosen non-collinearly. *Spicy* adopts the octahedral point charge model, where multipole moments up to quadrupoles are represented as

$$
\begin{aligned}
q_{(d_q,0,0)} &= \frac{Q_0}{6} + \frac{Q'_x}{2d_q} + \frac{Q'_{xx}}{3d_q^2} \\
q_{(-d_q,0,0)} &= \frac{Q_0}{6} - \frac{Q'_x}{2d_q} + \frac{Q'_{xx}}{3d_q^2} \\
q_{(0,\,d_q,\,0)} &= \frac{Q_0}{6} + \frac{Q'_y}{2d_q} + \frac{Q'_{yy}}{3d_q^2} \\
q_{(0,\,-d_q,\,0)} &= \frac{Q_0}{6} - \frac{Q'_y}{2d_q} + \frac{Q'_{yy}}{3d_q^2} \\
q_{(0,\,0,\,d_q)} &= \frac{Q_0}{6} + \frac{Q'_z}{2d_q} + \frac{Q'_{zz}}{3d_q^2} \\
q_{(0,\,0,\,-d_q)} &= \frac{Q_0}{6} - \frac{Q'_z}{2d_q} + \frac{Q'_{zz}}{3d_q^2},
\end{aligned}
\tag{14}
$$

with a small distance d_q, and Q' being multipole tensor elements expressed in the coordinate system of the principal axes of the Cartesian quadrupole tensor. These values are obtained from an arbitrary Cartesian quadrupole tensor $\boldsymbol{Q}_2$ through simple diagonalization

$$
\boldsymbol{R}^{\mathrm{T}}
\begin{pmatrix}
Q_{xx} & Q_{xy} & Q_{xz} \\
Q_{xy} & Q_{yy} & Q_{yz} \\
Q_{xz} & Q_{yz} & Q_{zz}
\end{pmatrix}
\boldsymbol{R} =
\begin{pmatrix}
Q'_{xx} & & \\
& Q'_{yy} & \\
& & Q'_{zz}
\end{pmatrix}
= \boldsymbol{Q}'_2.
\tag{15}
$$

The atomic dipoles $\boldsymbol{Q}_1$ must be rotated into the same axes system using $\boldsymbol{R}$:

$$
\boldsymbol{R}^{\mathrm{T}}\boldsymbol{Q}_1 = \boldsymbol{Q}'_1
\tag{16}
$$

Those DCMs introduce higher order multipoles for $d_q \neq 0$, which are usually negligible for small values of d_q such as the $0.25\,a_0$ as proposed by Gao.[87] The charge octahedron of Equation (14) is defined in the basis spanned by the principal axes of the Cartesian quadrupole tensor. A local molecular reference frame is required to rotate the octahedron, so that the multipole moments have the correct orientation relative to other nuclei. Following the approach of Devereux et al., a local reference frame may be constructed from triples of non-collinear atoms.[88] The algorithm to select an appropriate reference frame for atom f and up to two other atoms g and h (Figure 2) is outlined below:

1. If f has two directly bonded partners g and h, and $\boldsymbol{r}_{fg}$ and $\boldsymbol{r}_{fh}$ are not collinear, then $f = b$, $g = a$, and $h = c$. If they are collinear, choose another g and recurse.
2. If f has only one bond partner g, and g has another bond partner h and $\boldsymbol{r}_{fg}$ and $\boldsymbol{r}_{fh}$ are not collinear, then $f = a$, $g = b$, and $h = c$. If they are collinear, choose another h and recurse.
3. If f has only one bond partner g, and g has no other bond partner, look for the nearest neighbor h in the neighbor list of f, then $f = b$, $g = a$, and $h = c$. If they are collinear, choose another h and recurse.
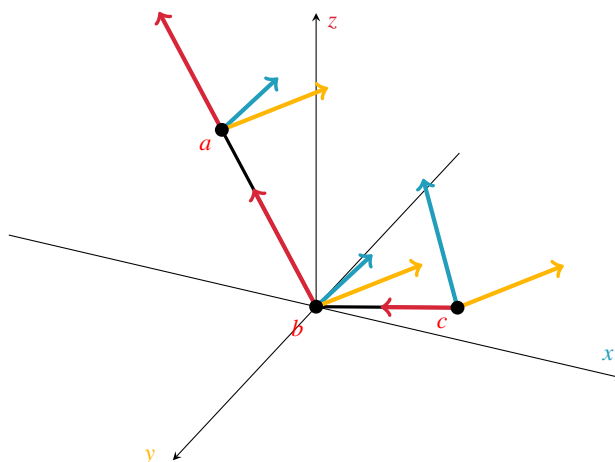
FIGURE 2 Reference frame and its axes systems for an atom triple a, b, and c. The axes labeled x, y, and z are the molecular Cartesian coordinate system in the Cartesian orthonormal basis. The blue, yellow, and red vectors are the basis vectors of the orthonormal basis, which is spanned by the principal axes of the Cartesian quadrupole tensor for each of the atoms a, b, and c, as in Equation (17). This local, atom-specific coordinate system is used to define the octahedral arrangement of point charges as in Equation (14).

4. If f has no bond partner, look for the two nearest neighbors of f in the neighbor list. If r_{fg} and r_{fh} are not collinear, then $f = b$, $g = a$, and $h = c$. If they are collinear, choose another h and recurse.
5. If f has no bond partner and only one neighbor g in the neighbor list, only one axis r_{fg} can be defined, which is invariant under rotation.
6. If f has no bond partner and no neighbor can be found in the neighbor list, the principle axes of the Cartesian quadrupole tensors coincide with the molecular coordinate system.
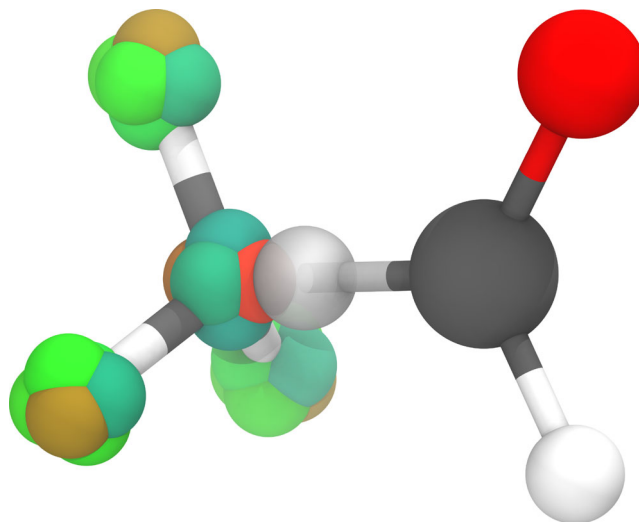
Each application of these rules assigns between one and three atoms to a reference frame. Doing so may assign multiple reference frames to the same atom. In those cases, only the first reference frame containing the atom is used. The basis vectors $o_{x,y,z}$ for the octahedral charge model of atoms a, b, and c, in the basis of the principle axes of the quadrupole tensor are obtained as

$$o_z^{a,b} = \frac{r_{ab}}{\|r_{ab}\|_2} \quad p_z^c = \frac{r_{bc}}{\|r_{bc}\|_2}$$

$$o_y^{a,b,c} = \frac{o_z^a \times o_z^c}{\|o_z^a \times o_z^c\|_2} \tag{17}$$

$$o_x^{a,b} = o_z^{a,b} \times o_y^{a,b,c} \quad o_x^c = o_z^c \times o_y^{a,b,c}.$$

Thus, the coordinates of the point charges C in the basis of the principal axes of the quadrupole tensor O for each octahedron can be transformed into the molecular coordinate system M, yielding $\overline{C}$:

$$\begin{aligned} O &= \begin{pmatrix} o_x & o_y & o_z \end{pmatrix} \\ M &= \begin{pmatrix} e_x & e_y & e_z \end{pmatrix} \\ C &= \begin{pmatrix} u_1 & \dots & u_6 \\ v_1 & \dots & v_6 \\ w_1 & \dots & w_6 \end{pmatrix} \\ \overline{C} &= M^T O C. \end{aligned} \tag{18}$$

FIGURE 3 Electronic embedding ONIOM2 setup for ethanal. Real system atoms $A_{()}$ are shown as sticks; atoms $A'_{(A)}$ belonging to the model system are shown using ball and stick representation. The transparent hydrogen link atom used in the model system is the only member of $A_{(A),l}$. In the calculations with theory levels $c_{()}$ (low) and $c_{(A)}$ (high) on node (A) (model system), the electric field from $A_{(),r}$ is approximated by the DCM. The small, colored spheres around the atoms of $A_{(),r}$ represent the point charges, comprising the DCM. Charge signs and magnitudes are indicated by a color code. Negative charges are blue, neutral charges green, and positive charges are shown in red. For illustrative purposes, hydrogen and carbon point charges use a different color scale.

$e_{x,y,z}$ usually are the Cartesian basis vectors and therefore $\boldsymbol{M} = \boldsymbol{E}$.

In contrast to the original algorithm outlined by Devereux et al.,[88] which only considers covalently bound systems, in ONIOM multiscale setups, also non-covalently bound systems have to be considered. The following example illustrates the problem: a protonated tertiary amine R_3NH^+ is in proximity to its bromide counter ion Br^-. The interaction is electrostatically dominated, and Br^- and R_3NH^+ are not considered bonded in the sense of ONIOM (which would imply the introduction of link atoms if the $R_3NH–Br$ bond is broken). Nevertheless, due to the high polarizability of the bromide, its electron distribution should not be isotropic. Instead, a non-zero dipole moment is expected to arise. This corresponds to case 4 in the algorithm above, resulting in the construction of a $Br–H–N$ reference frame. An important choice is the distance, up to which electrostatic interactions are still considered (see cases 3 to 5). Monopole–monopole interactions decay with r^{-1} and *Spicy* considers them negligible beyond 1.5 nm, as commonly done in classical MM simulations. Therefore, a neighbor list for distances of at least 1.5 nm is required. The resulting DCM, for an ONIOM2 calculation on ethanal, obtained from the algorithm just outlined, is shown in Figure 3.

In the context of arbitrary MC-ONIOMn, a polarization scheme for all subsystems has to be defined. This scheme should ideally allow reasonable polarization for arbitrary deeply embedded layers, while ensuring the independence of the different ONIOM tree branches. Building on the depth-first walk through the tree (as discussed in Section 2.1) that performs the calculations on each node, an embedding scheme for an arbitrary subsystem is defined as follows: The set of virtual embedding atoms for node (i) is called $A_{p,(i)}$, and the rules to construct this set define the embedding scheme.

$$A_{p,(i)} = \begin{pmatrix} A^{c_{(i:)}}_{(i:)} \smallsetminus A_{(i)} \cup A_{p,(i:)} & (i:) \neq () \\ A^{c_{()}}_{()} A_{(i)} & \text{otherwise} \end{pmatrix} \tag{19}$$

Here, $(i:)$ denotes a subsequence of (i), which is obtained by removing the last element of (i), and the superscript in $A^{c_{(i:)}}_{(i:)}$ means that the multipoles of these atoms are obtained by the original (high level) calculation of each layer. Therefore, Equation (19) defines a scheme, which walks a branch of the tree bottom-up, starting from the node of interest. All parent nodes in the branch of the node of interest contribute to its polarization, and the highest level multipoles available for each atom are used. Importantly, this scheme ensures that no inter-branch polarization between different nodes at the same level is encountered, allowing different branches to be calculated independently. To avoid over-polarization, a scaling function $s(N_b)$ can be applied to the atomic multipoles in set $A_{p,(i)}$, where N_b is the number of

bonds that separates any atom $a \in A_{p,(i)}$ from any other atom $b \in A_{(i)}$, while considering the shortest path between a and b.

2.3 | Fragment methods

Fragment methods offer an efficient approximation to fully quantum mechanical calculations while mitigating the steep scaling of the full system's description. Instead, they describe a chemical system in terms of smaller components or fragments, limiting individual quantum mechanical calculations to systems of feasible size. Originally, the combination of the MBE with ONIOM has been proposed as *generalized ONIOM*, to reduce the computational costs of ONIOM calculations with large QM layers.[60] A multitude of fragment methods exist in the literature, such as the MBE,[90] GMBE,[61] systematic molecule fragmentation (SMF),[91] systematic molecule fragmentation by annihilation (SMFA),[92] FCR,[62] and molecular fractionation with conjugated caps (MFCC).[93] Given a MBE truncated at n-mers, the calculation time scales linearly with the number of groups in the system for a fixed n, if an interaction cutoff is introduced. Among those fragment methods, GMBE and FCR are the most general, as they place no restrictions on the fragment composition. In *Spicy*, a combination of methods from SMFA, GMBE, and FCR is employed to define a rather general fragmentation scheme. Fragment methods may be used instead of a monolithic calculation for any node in the MC-ONIOMn tree. Applied to the large outer layers, this allows building ONIOM setups, where even the lower level outer layers can be treated quantum mechanically in an economic fashion.

Below, the implementation of fragment methods in *Spicy* is outlined. Given a set of atoms A, it can be partitioned into groups $G = \{g_1, g_2, ..., g_n\}$, where each group is a set subset of the atoms $g_i \subset A$, and

$$
\begin{aligned}
g_i \cap g_j &= \emptyset, i \neq j \\
\bigcup G &= A.
\end{aligned}
\tag{20}
$$

A molecule can be represented as an undirected graph, with the atoms A being labeled vertices, and bonds being labeled edges. Atom labels include a formal electronic charge and a formal number of unpaired electrons in the α and β orbitals. Bond labels are an abstract bond order, which is either a *single* bond, a *multiple* bond (any bond with a bond order > 1), or a *coordinative* bond.

Spicy employs a slightly extended version of the SMF rules for group generation, to obtain bond orders and groups, as outlined below.[92]

1. Initially, all atoms/vertices of the molecular graph are disconnected (Figure 4a). Bonds/edges, labeled with the abstract bond order, are introduced by the following steps:
   a. If $d_{ab} \leq R_a^{cov} + R_b^{cov} + d_m$, ($d_m < d_s$, usually $d_m = 7pm$), and the number of bonds both a and b have, indicate a subvalent pair, their bond order is changed to *multiple*. Common valencies are looked up from a valency table for each element.
   Each bond label may be overwritten by the user. Finally, a molecular graph with atom vertices and undirected, labeled bond edges is obtained (Figure 4b).
   b. If a and b were connected through 1a, and any of the atoms a and b is a metal,* their bond label is changed to *coordinative*.
   c. If $d_{ab} \leq R_a^{cov} + R_b^{cov} + d_s$, where d_{ab} is the distance between two atoms a and b and d_s is an additional tolerance (usually $d_s = 40pm$), a and b share a *single* bond.
2. All *single* bonds that do not involve a hydrogen atom are deleted from the graph. The disconnected subgraphs are preliminary groups, and within each preliminary group, the sum of the formal charge and the formal number of unpaired electrons is checked. If any of both is non-zero, all group members' bonds are added again. This means that charged or spin-polarized preliminary groups assimilate their neighbors. The disconnected subgraphs resulting from this step are the final groups (Figure 4c).
3. The molecular graph is reduced to an undirected graph of groups (Figure 4d). The labeled vertices are the groups g_i, and unlabeled edges represent the original connections of the groups.
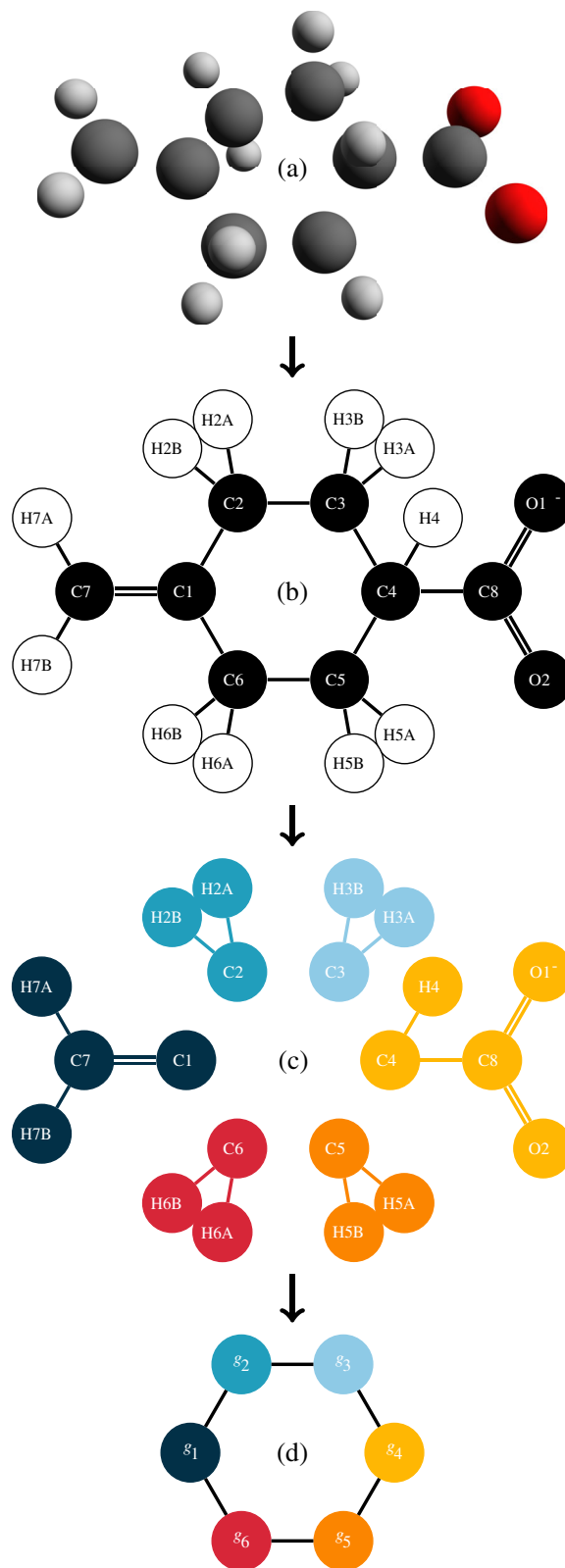
FIGURE 4 Partitioning procedure of a molecular graph, yielding groups $G = \{g_1, g_2, ..., g_n\}$. In the initial physical system description (a), the molecule is described by A in $\mathbb{R}^3$ without bond information. Bonds and their abstract orders are guessed via modified SMF rules, allowing the graph representation (b). Preliminary disconnected subgraphs are formed by deleting all single bonds that do not involve hydrogen. Preliminary groups that are charged or spin-polarized (according to the label information of the atoms) are reconnected to their direct neighbors, and the final subgraphs/groups (c) are obtained. A simplified graph of groups can be constructed, by maintaining the overall topology, but dropping the edge labels (d).
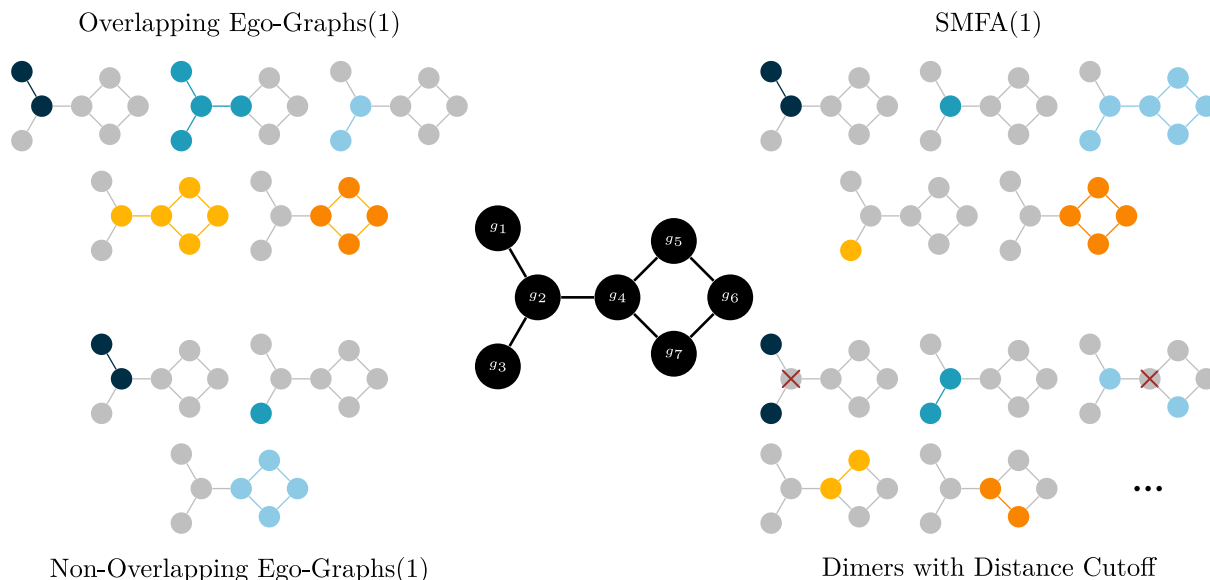
FIGURE 5   Different algorithms to generate fragments from a graph of groups (center). Fragments are shown as color-coded nodes. Nodes not part of a fragment are shown in gray. Overlapping ego-graphs (top left) of length 1 for each group yield strongly overlapping fragments. The ring-avoidance rule prevents formation of the problematic fragments $\{\{g_2, g_4, g_5, g_7\}, \{g_4, g_5, g_6\}, \{g_5, g_6, g_7\}, \{g_4, g_7, g_6\}\}$. Non-overlapping ego-graphs (bottom left) of length 1 exclude each group, that has already been assigned to a fragment from further inclusion in other fragments. Thus, those fragments do not overlap. The ring-avoidance rule is also applied for non-overlapping ego-graphs, and the fragment $\{g_4, g_5, g_6, g_7\}$ instead of $\{g_4, g_5, g_6\}$ is formed. SMFA (top right) applies a recursive elimination scheme of groups and reduces the fragment size down to a given size threshold. Fragments may also be formed by n-combinations of groups or other fragments. The bottom right shows the small subset of fragments, obtained when 2-combinations of the groups are formed. Many of such dimers may include problematic interactions of link atoms, if the groups are small. When $\{g_1, g_2, g_3\}$ is a prop-2-yl group, the dimer $\{g_1, g_3\}$ would introduce link atoms in close proximity to each other (marked by red $\times$), and similar for the dimer $\{g_2, g_7\}$.

The graph of groups is the basis to construct a set of fragments $F = \{f_1, f_2, ..., f_n\}$. The fragments (*auxiliary monomers* in the language of GMBE) are defined in terms of groups and may arbitrarily overlap but must comprise the entire graph.

$$f \subseteq G$$
$$f_i \cap f_j \subset G, i \neq j$$
$$\bigcup F = G$$

(21)

Different algorithms, which may or may not make use of connectivity of the graph of groups, can be used to generate fragments in terms of groups (Figure 5).

Spicy implements SMFA, two types of graph traversals with ego-graphs, and fragment construction from n-combinations of groups or fragments, generated from graph-traversal or SMFA. The ego-graph of length l around a given vertex is a subgraph of the original graph, where all the subgraph's vertices can be reached with a maximum of l steps along the edges, starting from the given vertex. Each vertex in the graph of groups is visited, and its ego-graph of a specified length is formed to construct fragments. Similar to the level in SMFA, the length of the ego-graph l acts as an accuracy parameter of the fragmentation method, as does n, when forming n-combinations. The top left approach in Figure 5, constructs the ego-graph for every node, regardless of whether the node is already part of a fragment, resulting in overlapping fragments. A second fragmentation approach removes any vertex from the graph of groups that has been assigned to a fragment before processing the next vertex, producing non-overlapping fragments. Problematic fragmentations that suffer from unphysical interactions can occur when a single, small group such as $-CH_2-$ is removed from a cyclic structure of the graph. To circumvent such cases, a ring avoidance rule has been implemented for SMFA and

ego-graph-based constructions, avoiding fragmenting rings of size $2n+2$, where n is the level of SMFA, respectively the length of the ego-graphs.[91,92] Figure 5 contains an example where the ring-avoidance rule prevents deconstructing the four-membered ring. The different fragment construction algorithms have different strengths and weaknesses. Graph-traversal approaches such as SMFA and ego-graphs construct spatially strictly confined fragments, where each fragment only contains directly bonded groups. Graph-based fragmentation allows for computationally very efficient fragment construction and their number grows only approximately linearly with the system's size. Conceptually they are well suited to describe the covalent interactions of a molecule, but miss non-covalent interactions. Groups with a large distance in the graph of groups can have a small distance in real space, and the graph-based approaches necessarily miss those. For example, in Figure 5, long-range interactions between the cycle and the substituents on the left part would not be included. The n-combinations of groups are better suited for inclusion of non-covalent interactions and they may also include combinations of groups that are distant in the graph but close in real space. Yet their construction is computationally more demanding due to the large amount of possible combinations, and their number grows fast with the system size. Employing very small groups, for example $-CH_2-$, as commonly constructed by SMF's group generation, can give rise to fragments with link atoms in very close proximity (see the first dimer in Figure 5). Link atoms that are too close, can introduce artificial unphysical repulsion between fragments and may prevent the convergence of QM calculations. This problem is avoided by using larger groups, such as whole amino-acid residues in a protein, or by forming n-combinations of non-overlapping ego-graph fragments. *Spicy* allows forming n-combinations of fragments, generated by one of the other methods while allowing to specify a cutoff distance, beyond which the n-combinations of involved groups will not be formed. The distance between a pair of groups g_a and g_b is $d_{g_a g_b}$. It is defined as the minimal distance between any of their atoms.

$$d_{g_a g_b} = \min_{\substack{i \in g_a \\ j \in g_b}} \left\| \boldsymbol{r}_{ij} \right\|_2 \tag{22}$$

Similar to the isolation of a sublayer in ONIOM, fragment construction is likely to leave dangling bonds in the fragments. Those are treated on the same footing as ONIOM subsystems, that is, the bonds are capped with link atoms, as shown in Equations (1) and (2).

Originally, the GMBE provided an expression to obtain the energy for a set of arbitrarily overlapping fragments but it also applies to any extensive property P. Each fragment f in the initial set of fragments F contributes an intersection-corrected property $\overline{P}(f)$ to the full system's property $P(F)$ in terms of its constituting fragments.

$$
\begin{aligned}
P(F) = & \sum_{a=1}^{|F|} \overline{P}(f_a) \\
\overline{P}(f_a) = & \ P(f_a) - \sum_{bb>a}^{|F|} P(f_a \cap f_b) \\
& + \sum_{b,cc>b>a}^{|F|} P(f_a \cap f_b \cap f_c) \\
& - \ldots \\
& + (-1)^{|F|-a} P\left(f_a \cap f_{a+1} \cap \ldots \cap f_{|F|}\right)
\end{aligned}
\tag{23}
$$

The GMBE equation applies universally to any set of fragments and ensures that double counting is avoided by the principle of inclusion and exclusion.[61,62] Again, a graph-theoretical approach can be used to implement Equation (23) which can be viewed as a forest of trees that form intersections (Figure 6). Each tree represents the calculation of an intersection-corrected property by forming intersections of fragments from the original set, until the intersections become empty. The depth of a node in each tree determines the sign in the GMBE sum, starting with a positive sign, and then alternating for each layer in each tree of the forest.

The implementation of the GMBE sum as a forest is concisely formulated as hylomorphism of trees. While unfolding the trees (anamorphism), fragments f' arise that were not necessarily part of the original fragment set F, and their properties must also be calculated. A consistent electronic structure is ensured by annotating the groups with
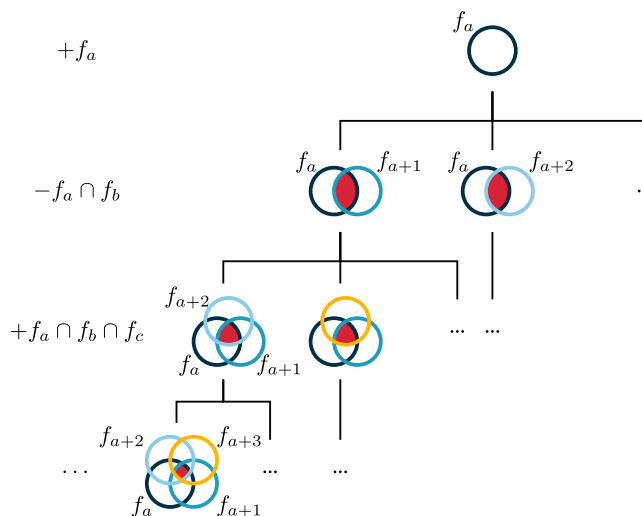
FIGURE 6   A tree can be used to represent an intersection corrected property $\overline{P}$ from Equation (23). The circles represent fragments f_i from the initial set of fragments F, and the color encodes the actual fragment. Intersections of those fragments are marked in red, and a branch of the tree terminates when an intersection becomes empty. The depth of a node in the tree n determines the sign with which the fragment that is obtained by this node contributes to the GMBE sum as $(-1)^n$, and denotes that $n+1$ fragments intersect.

additional information such as charge and spin. This also allows different magnetic couplings between groups to be considered. Implementing GMBE as an anamorphism gives rise to a myriad of terms, resulting in very large trees, especially with strongly overlapping fragments, for example, whenever n-combinations are formed. However, most terms cancel when collapsing the trees and summing over the different signs (catamorphism). Calculating the GMBE can become tremendously demanding, and calculating the GMBE sum for dimers of only ≈ 100 groups can become nearly impossible. In practice, this hylomorphism becomes the bottleneck of GMBE calculations, way before the QM calculations. The FCR formalism recently introduced by Hellmers and König,[62] provides an alternative approach to express and implement GMBE. $R(F)$ is the set of all fragments that may be formed from the original set of fragments F in terms of the power sets $\mathcal{P}$ of the individual fragments:

$$R(F) = \bigcup_{f \in F} \mathcal{P}(f) \tag{24}$$

This new set R is called the fragment combination range, and provides an alternative way to write the GMBE sum over extensive properties

$$P(F) = \sum_{\substack{s \in \mathcal{P}(r) \\ r \in R(F)}} (-1)^{|r|-|s|} P(s). \tag{25}$$

A formulation in terms of FCRs has the advantage to be independent of the overlap of fragments, which needs to continue until empty sets of groups are encountered and avoids the unfavorable growth of the trees as in Equation (23) and Figure 6. By avoiding recursion over sums in Equation (25), the number of terms in the GMBE is reduced dramatically. In consequence, the required computation time grows only linearly with the number of fragments in the original set for a given fragmentation scheme, and much larger systems can be treated using the FCR formalism.

The computational aspects of GMBE can be improved when approximate fragment interactions are included via electronic embedding. While arbitrary long-range interactions could be taken into account, the number of required computations increases drastically with growing distance cutoff during the n-combinations of groups and fragments. Instead, these long-range interactions can be approximated by electronic embedding, which even allows decreasing the distance cutoff. Contrary to the electronic embedding of ONIOM layers, the fragments have no hierarchical order, and polarization does not occur unidirectionally, as the fragments influence each other. Embedding multipoles for each

fragment can either be obtained from gas-phase calculations on each fragment in R or in a self-consistent manner in the spirit of the X-Pol method.[63] In X-Pol, the multipoles for a given fragment are iteratively calculated in the field of the other fragments of the previous iteration until the residual mean square value of all atomic multipoles converges to a certain threshold. Due to the absence of density-matrix derivatives for the multipole moments, those contributions are neglected, but the resulting errors were found to be very small.[63] Each atom a may appear in multiple fragments, and, thus, several multipoles may be available for each atom. *Spicy* follows Richard's and Herbert's suggestion, that each atom's atomic multipoles should be arithmetically averaged over the different fragments.[61] Typically, the atomic multipoles in a X-Pol approach converge in <10 iterations.

2.4 | Optimizations

Direct geometry optimization of an entire ONIOM system is not different from optimizing a non-ONIOM system. Both MC-ONIOMn and GMBE provide gradients and Hessians (Equations (13) and (25)), enabling usage of standard second-order optimization algorithms. However, for large systems, direct optimizations can become prohibitively expensive. First, Hessian diagonalization for a system comprising N atoms scales as $\mathcal{O}(N^3)$, which can outweigh the costs to calculate the system's energy and gradient. This can, in principle, be solved by using optimizers that do not utilize Hessian information (conjugate gradient[94]) or avoid construction of the Hessian explicitly (limited memory Broyden–Fletcher–Goldfarb–Shanno (L-BFGS)[95]). Second, the internal-Cartesian back-transformation can become expensive for large systems as it can involve multiple $\mathcal{O}(N^3)$ steps. And third, weakly bound systems and molecular clusters may be difficult to converge, and often require care in the coordinate setup or specialized fragment coordinates.[96] For multilayer schemes like QM/MM and ONIOM, the consequence is often that a large number of expensive optimization steps is required. While outer layers commonly use semiempirical or MM methods, where gradients are inexpensive to calculate, they often contain weakly interacting fragments or solvent molecules which require many steps until a stationary point is obtained. At the same time, the costs to evaluate the gradient of the entire ONIOM setup are often dominated by the inner layers, which may require only a few optimization steps but commonly employ expensive ab initio methods. The problem has long been recognized and was solved by algorithms that utilize micro-cycles, where the outer layer is optimized before taking a step in the inner layer.[97,98] In *Spicy*, we generalize micro-cycle driven geometry optimizations to arbitrary MC-ONIOMn setups while further disconnecting the optimization steps on different layers.

To optimize a layer (i) independently from its sublayers, a subset $\boldsymbol{q}_{(i)} \subseteq \boldsymbol{q}$ of the coordinates of the entire system $\boldsymbol{q}$ must be chosen. Changing the coordinates $\boldsymbol{q}_{(i)}$ must not influence the nuclear gradients of any layer that is not a parent layer

$$\frac{\partial E_{(j)}}{\partial \boldsymbol{q}_{(i)}} = \boldsymbol{0}, (j) \neq (i) \wedge \forall \,|(j)| \geq |(i)|. \tag{26}$$

Consequently, for a given layer (i), $\boldsymbol{q}_{(i)}$ must comprise the coordinates of atoms that are exclusively members of this layer. In addition, the coordinates of the link atom hosts in the parent layer must be included, whose missing valencies are mimicked by link atoms (see Figure 7).

However, for MC-ONIOMn, the situation is complicated, as two or more sublayers of a layer may have link atoms $a_l^{(A)}$ and $a_l^{(B)}$ that share the same link host atom $a_h^{()}$. During nuclear displacement steps, both subsystems contribute to the gradient and therefore displacement step of $a_h^{()}$, influences properties of both subsystems (see Figure 8).

Thus, to account for possible couplings between subsystems, these subsystems must be optimized simultaneously. However, the calculations on centers of the same depth slice can still be performed independently. Consequently, valid micro-steps for an ONIOM tree can be taken in all cases if layers in the same horizontal slice D_d are optimized simultaneously and Equation (26) is instead written as

$$\frac{\partial E_{D_d}}{\partial \boldsymbol{q}_{D_e}} = \boldsymbol{0}, e > d. \tag{27}$$
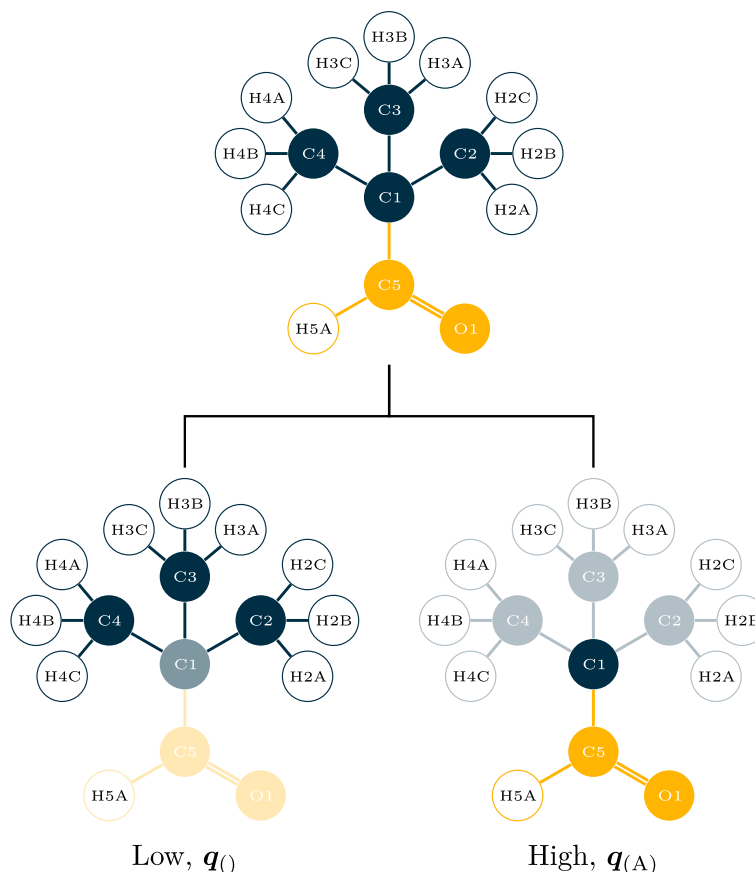
FIGURE 7 Separation of coordinates for 2,2-dimethylpropanoic acid in an ONIOM2 setup. The high-level layer comprises the carboxy group (yellow), and the low-level layer also comprises the *tert*-butyl group (blue). To satisfy the condition $\partial E_{(A)}/\partial \boldsymbol{q}_{()} = \boldsymbol{0}$, $\boldsymbol{q}_{()}$ must not include coordinates of C1, as coordinates of the link atom in the model system directly depend on those of C1 (Equations (1) and (2)).
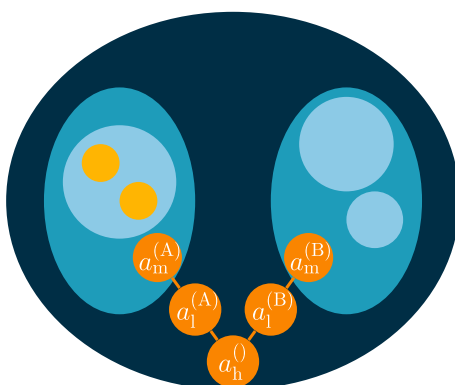
FIGURE 8 The MC-ONIOM4 setup from Figure 1, where the layers (A) and (B) couple indirectly through a common link host atom in the layer (). In this example two atoms of the model systems $a_m^{(A)}$ and $a_m^{(B)}$ are capped by the link atoms $a_l^{(A)}$, respective $a_m^{(B)}$, and the coordinates of both link atoms depend on the coordinates of $a_h^{()}$. Thus, the condition from Equation (26) can only be satisfied, if $\boldsymbol{q}_{(A)} = \boldsymbol{q}_{(B)}$, which can be satisfied if (A) and (B) are optimized simultaneously (Equation (27)).

It is possible to use a different optimization strategy for each depth-slice of the ONIOM tree if care is taken that translational and rotational degrees of freedom are correctly accounted for. An advantage of this separation is, that different coordinate systems can be used for optimizing different slices, that is, translation rotation internal coordinates (TRIC)[96] or simple Cartesian coordinates for the large, outer layers, and redundant internal coordinates for the inner layers. Furthermore, an optimizer only treating a small inner layer can optimize to a transition state without interference from

modes of outer layers.[99] An algorithm, suitable for such a micro-cycle driven optimization with independent optimizers for each depth slice is outlined below:

1. Setup coordinates $\boldsymbol{q}_{D_d}$ for each depth d according to Equation (27). Layers at the same depth slice will be optimized simultaneously.
2. Initialize a separate optimizer for each depth slice and specify a coordinate system, convergence threshold, and optimization algorithm. All atoms $A_{()}$ and their coordinates $\boldsymbol{q}$ are visible to each optimizer so that translational and rotational degrees of freedom are correctly handled. However, all coordinates except $\boldsymbol{q}_{D_d}$ are frozen for an optimizer at depth d. In the construction of internal coordinates, frozen atoms can be excluded, thus keeping the number of defined internal coordinates to a minimum.
3. Calculate the MC-ONIOMn gradient for the full system.
4. Initialize depth d to start at the deepest slice of the MC-ONIOMn tree, thus $d = n - 1$.
5. Optimize $\boldsymbol{q}_{D_d}$ by performing the following steps:

a. If $d < 0$ return.
b. Request slice D_{d-1} to be completely optimized by recursively calling into step 5 with $d - 1$.
c. Calculate the gradient of all slices $D_{i \leq d}$ to obtain a valid gradient expression for $\boldsymbol{q}_{D_d}$.
d. Calculate and perform a geometry displacement step in $\boldsymbol{q}_{D_d}$.
e. Check for the convergence in $\boldsymbol{q}_{D_d}$. If the optimization at this depth slice has converged, return. Otherwise recurse into step 5a.

Thus, every depth slice requires all parent depth slices to be fully optimized before performing a single geometry optimization step. When the optimizer returns, the deepest depth slice has converged, ensuring that all slices above have also converged.

Equation (27) is only strictly satisfied for mechanical embedding. In electronic embedding schemes, the displacement of atoms in parent slices will always affect the properties of sublayers through the electric field, polarizing the sublayers. As has been previously shown, it is necessary to take the change of the embedding charges with respect to the nuclear coordinates into account to calculate valid gradients with electronic embedding.[100] For DMA such nuclear derivatives have not been formulated yet, and our implementation must therefore ignore these small contributions, possibly at the expense of requiring more optimization steps. In contrast to electronic embedding schemes in QM/MM, where the QM part and MM part polarize each other, and another set of microcycles has to be performed,[97] the unidirectional nature of electronic embedding in ONIOM simplifies the problem. The algorithm outlined above also ensures that steps are always taken in the presence of a consistent polarizing electric field.

3 | IMPLEMENTATION

The *Spicy* program is written as a platform to develop, test, and implement ONIOM and fragment methods, available on GitLab (https://gitlab.com/theoretical-chemistry-jena/quantum-chemistry/Spicy), and licensed under the free AGPL-v3. *Spicy* is implemented in Haskell, which allows a very high-level programming style without sacrificing performance. Haskell's cheap green threads and software-transactional memory allow a heavily asynchronous programming style with a clear separation of tasks (e.g., see Sections 3.1 and 3.2).[101] Furthermore, the "massiv" array library, also building on Haskell's green threads, enables parallel and efficiently fused array operations.[102]

For example, construction of local frames and the DCM comprises only a minor part of the calculation time. The rules outlined in Section 2.2 to select a suitable reference frame can be efficiently checked by utilization of a neighbor list that is obtained in $\mathcal{O}(N)$ for N atoms and that is subsequently also used to determine the system's topology. Both the neighbor list and the topology are stored as a PATRICIA tree of the atom indices and provide efficient lookups in $\mathcal{O}(\min(N, W))$ with $W = 64$.[103,104] Consequently, construction of the embedding charges comprises typically $< 1\%$ of the runtime costs.

While still in early stages of its development, *Spicy* already implements arbitrary non-overlapping MC-ONIOMn (Section 2.1), electronic embedding with distributed multipole expansions up to the quadrupoles (Section 2.2), the GMBE in terms of FCR together with a set of fragment generation algorithms (Section 2.3), direct and micro-cycle driven optimizations, a couple of interfaces to external computational chemistry programs (Section 3.1), and a VMD-

inspired[105] selection language for layer and fragment setups. Emphasis is put on a general implementation that exposes important tuneable parameters and which avoids implementing special cases for specific layouts or method combinations.

3.1 | Interfaces to quantum chemistry programs

Spicy interfaces a couple of computational chemistry programs which are utilized to perform individual subsystem calculations. Interfaces to the xTB program,[106] Psi4,[107] and Turbomole[108] are currently available, offering access to all methods available in these programs. As most computational chemistry programs do not offer a C-application programming interface (API) or cannot easily be wrapped with a C-API, file-based interfaces are often required, an approach commonly taken by external interfaces.[46,47,68,96,109] Both input generation for external programs and output handling from the external sources are unified in common data types in *Spicy*. The common input data type allows specifying computational models, convergence options, and approximations in a structured data type. However, the definition is general enough to access arbitrary methods of the underlying computational chemistry engines. Another data type stores the calculation results from the external programs and comprises energies and nuclear derivatives thereof, distributed multipole moments, the orbital basis, and a one-particle density matrix or wavefunction. Multipole moments for quantum mechanical calculations are automatically obtained by passing the appropriate data to Stone's GDMA program[66] as formatted checkpoint files (.fchk). These formatted checkpoints are serialized from *Spicy's* unified data structures and thus enable the GDMA program to be used with programs that do not natively produce formatted checkpoint files.

Spicy requests subsystem calculations from an asynchronous calculation backend in a concurrently running thread, clearly separating the logic of ONIOM and fragment methods from the work to obtain required physical data. Calculation requests are queued, and the backend orchestrates the calculations. Furthermore, it allows extending the calculation backend to a network-distributed scheduling system, scattering the calculations over multiple machines, for example, on a high-performance-computing cluster.

3.2 | i-PI client and optimizations

Similar to the calculation of subsystems' properties (Section 3.1), *Spicy* does not implement the optimizers itself but interfaces external, well-tested, and proven engines. The i-PI path integral MD engine[110] uses a network-based communication protocol, which requests force evaluations from a computational chemistry program and provides new geometries to those clients based on a time propagation step. A superset of the original, client-sided protocol has been implemented in *Spicy*, which adds additional communication options to exchange Hessians and energies. The extended protocol is a superset, strictly compatible with the original implementation. *Spicy* interfaces the pysisyphus optimization engine[68] via this extended i-PI protocol, giving full access to pysisyphus' optimization algorithms and allow searching stationary points (minima and first-order saddle points) in internal and Cartesian coordinates. Pysisyphus is also used in micro-cycle driven optimizations, where one i-PI client thread per depth slice of the ONIOM tree is utilized. The very low costs of green threads and low latency, high bandwidth UNIX sockets ensure high efficiency in this asynchronous calculation model.

The i-PI protocol and *Spicy's* asynchronous communication model will also facilitate the integration of molecular dynamics engines.

3.3 | Package composition and build system

Spicy is written in standard Haskell2010[111] with a common set of extensions and Haskell dependencies and uses the Cabal build system. Thus, *Spicy* is a fairly standard and portable Haskell package. A test suite is regularly executed by continuous integration, fully statically linked build artifacts are available, and dependencies are updated regularly.

However, due to reliance on large computational chemistry packages, the dependency graph for an actual *Spicy* runtime is rather large and complex, comprising 211 Haskell and 360 non-Haskell dependencies at the moment. Installing and satisfying all dependencies is an additional challenge in software stacks that mix different ecosystems, such as C/C++, Fortran, Python, and Haskell. Additionally, composing a working runtime environment can be complicated by conflicting versions of MPI or BLAS/LAPACK implementations and more. Consequently, reproducing a

computational environment at a different point in time or on a different machine is extraordinarily difficult. *Spicy* can optionally be built with Nix, a purely functional software management system aiming at full reproducibility.[112] By integration of nixpkgs and the NixOS-QChem overlay, *Spicy* and all its dependencies, including the computational chemistry programs, can be built fully reproducible, ensuring perfect transferability.[113–115]

4 | TESTS AND APPLICATIONS

In scientific software, implementation errors can be particularly insidious; they can manifest as hard to detectable numerical errors, especially since reference values may simply not be available for new methods. For this reason, *Spicy* includes a suite of unit- and property tests which ensures that key parts of the ONIOM code exhibit correct behavior, as well as a selection of test calculations to check the proper interaction between *Spicy* and its calculation providers. These test suites are distributed with *Spicy* and can be automatically executed through the Nix and Cabal build systems.

4.1 | Verification tests

Spicy has been tested on a variety of chemical systems to cover several methods and use cases. Some of these tests feature new systems while others ensure consistency with previous results and implementations. Several test cases are presented in the following. If not specified otherwise, calculations were performed using the standard settings of the involved programs. In particular, geometries were converged using the following criteria: absolute maximum force $\leq 4.5 \times 10^{-4} E_h a_0^{-1}$, root mean square (RMS) of all forces $\leq 3.0 \times 10^{-4} E_h a_0^{-1}$, absolute maximum displacement $\leq 1.8 \times 10^{-3} a_0^{-1}$, RMS of all displacements $\leq 1.2 \times 10^{-3} a_0^{-1}$.

In their article accompanying the implementation of ONIOM3 in Gaussian,[54] Dapprich et al.[78] present a set of geometry optimizations. These calculations on ethanal, trifluoroethanal, propanal, and cyclobutene have been reproduced in *Spicy*, using Psi4[107] as the calculation provider. Reassuringly, results show excellent agreement between both implementations. Bond lengths and angles are accurately reproduced (see Table 1; Scheme 1). Minor differences are easily reconciled due to the fact that the original calculations used a non-standard modification of the B3LYP

TABLE 1 Deviations of selected parameters between spicy and literature for the optimized geometries of the test systems introduced by Dapprich et al.[78]

Molecule	Parameter	Lit.	Spicy	Δ
Ethanale	R_1	153.5	154.5	+1.0
	α	120.4	120.9	+0.5
	β	123.8	124.2	+0.4
Propanale	R_1	155.9	157.1	1.2
	R_2	155.3	155.2	−0.1
	α	120.5	121.1	+0.6
	β	123.3	123.7	+0.4
	γ	106.7	106.8	+0.1
	δ	112.8	112.8	0.0
Trifluoroethanale	r	159.7	166.1	+6.4
	α	123.2	123.8	+0.6
	β	121.5	122.0	+0.5
Cyclobutane	R_1	136.6	134.8	−1.8
	R_2	153.8	153.9	+0.1
	α	133.3	133.5	+0.2
	β	93.4	93.6	+0.2

Note: Parameter names refer to the labels in Scheme 1. Distances are in picometers, angles in degrees.
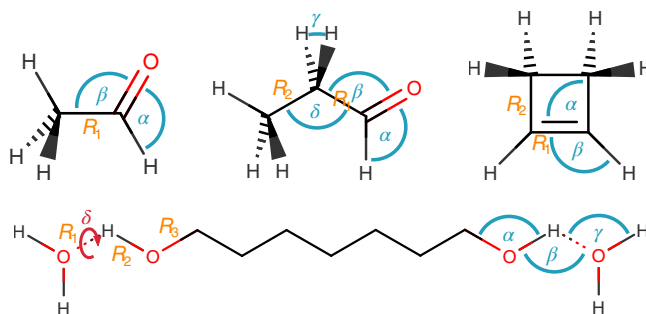
SCHEME 1 Test systems for geometry optimizations adapted from Dapprich et al.[78] (upper row) and Hopkins et al.[59] (bottom). The labeled bond lengths, angles and dihedral angles are compared with the literature reference (Drappich) or a non-ONIOM reference (Hopkins) in Tables 1 and 2.

TABLE 2 Comparison of selected parameters from the optimized geometries of the test systems introduced by Hopkins et al.[59]

Parameter	Model 0[a]	Model 1[a]	Model 2[a]	Ref.[b]
R_1	185.5	187.9	187.8	188.9
R_2	97.7	97.2	97.2	97.2
R_3	141.1	140.8	140.8	140.8
α	109.1	108.6	108.6	108.6
β	168.0	167.9	167.9	166.5
γ	105.1	104.9	104.9	103.6
δ	56.6	56.9	56.0	56.6

Note: Parameter names refer to the labels in Scheme 1. Distances are in picometers, angles in degrees.
[a]"Model *n*" refers to a model system that includes the water molecule, hydroxyl group, and *n* CH_2 groups along the alkane chain.
[b]Refers to a non-ONIOM calculation.

density functional as well as the unpolarized double-zeta basis DZV, both of which are not available in Psi4. Instead, the standard definition of B3LYP[116] was used and DZV was replaced with cc-pVDZ.[117]

Further, Hopkins et al.[59] introduced a cluster of 1,7-heptanediol and two hydrogen-bonded water molecules as a system to examine MC approaches. With Spicy, we have used this arrangement to demonstrate the accuracy of our MC-ONIOM scheme. Different model systems show little deviation from a conventional high-level calculation. Even small model layers appear well-suited to describe hydrogen-bonding interactions (see Table 2).

Vreven et al.[98] implemented a micro-cycle based optimization scheme to reduce the number of expensive QM calculations in geometry optimizations. To verify our own implementation, the systems examined in their work were optimized with *Spicy*. While a direct comparison is impossible due to missing methodical details in the original work, we are pleased to report that our micro-cycle optimization scheme is able to converge all systems in a small amount of QC steps: a water dimer (GFN-2[118]:MP2[119]/cc-pVDZ[117]) could be converged in as few as five steps, while hexaphenylethane (GFN-2:MP2[119]/cc-pVDZ) needed only seven steps. The highest number of steps were needed for a carbene with 18 steps. On the other hand, using the macro-cycle based approach incurs many additional calculations: the water dimer converges in 39 steps, while the carbene requires 62 steps. Hexaphenylethane required 14 steps until convergence, which is still a 100% increase from the more efficient micro-cycle scheme.

To further demonstrate the appeal of micro-cycle driven optimizations, we introduce a more challenging test system: a water/ammonia cluster arranged around a sulfate dianion. Optimization was carried out in TRIC[96] using a rational function optimizer (RFO) routine. This system is divided into two layers (GFN-2[118]:B3LYP[116]/def2-SVP[120]), with the sulfate anion comprising the inner layer. The system comprises 30 molecules and 103 atoms which have been assembled in a random orientation. The initial cluster is far away from its minimum energy structure. Compared with the previously discussed examples, this optimization is much more difficult, due to many shallow minima on the potential energy surface of solvated systems. Using the straightforward macro-cycle based approach, this system converges in 99 steps, requiring an equivalent amount of QM gradient evaluations. When using the micro-cycle driven procedure,
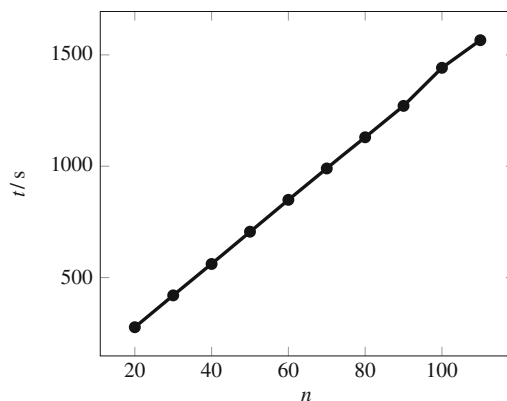
FIGURE 9 Total wall time costs t of a fragment calculation in spicy with respect to the number of methylene groups in a linear alkane $CH_3–(CH_2)_n–CH_3$.

the cluster geometry converges within 11 steps in the inner layer and 230 cycles in the outer semiempirical layer, yielding a tremendous reduction of potentially expensive QM calculations of 89%. In this example, a speedup of around 300% (201 s versus 600 s) could be achieved on a local workstation with a Intel Xeon W-2223 processor.

We conclude that *Spicy's* micro-cycle driven optimizations are an excellent tool to reduce computational effort during ONIOM geometry optimization.

Another set of original calculations examines the validity of the GMBE approximations as implemented in *Spicy*. For this, a cluster of 25 water molecules was chosen, as the individual molecules make natural fragments and also have pronounced multipoles to heighten the importance of charge embedding. The system was treated at the GFN-2 level of theory.[118] Using GMBE truncated at the dimer level without any charge embedding incurs an error of 186mE_h for a relative error in the GFN-2 energy below 0.15%. Introducing multipoles through an X-Pol scheme[63] reduces the error to 68mE_h (0.05% relative error) but requires an iterative scheme which, in this case, converges in six iterations. Using gas phase multipoles instead gives nearly identical results (within 2.4mE_h of the X-Pol method) while requiring only one additional calculation. Higher accuracy could of course be achieved by extending GMBE to include trimers.

Finally, a geometry optimization of cyclohexane demonstrates the robustness of the GMBE approach. Cyclohexane is fragmented using the overlapping ego-graph algorithm with length 1, leading to propane fragments. Despite its simplicity, this scheme performs very well, with all bond distances being replicated in sub-pm accuracy when compared to a non-GMBE calculation with the same method. Bond angles are also of high quality, with a RMSD of only 0.1 when compared to the non-GMBE reference.

To evaluate the scaling behavior of Spicy's fragment method implementation, a series of gradient calculations on a n-alkane of increasing chain length were conducted. Utilizing the SMF group generation discussed in Section 2.3, methyl and methylene groups are obtained. Fragments are then generated in a two-step procedure. First, non-overlapping ego-graphs of length one are constructed resulting in $CH_3–CH_2–$ and $–CH_2–CH_2–$fragments. In a second step, dimers of these preliminary fragments are formed within 750. Figure 9 illustrates the wall times of RI-MP2/cc-pVTZ calculations with respect to the size of the molecule. The wave function calculations were provided by Psi4 1.6.1[107] running on an Intel Xeon W-2155 CPU.

Clearly, Spicy can achieve linear scaling in this case. For $n = 20$ the cost of a standard MP2 calculation was already 1774 s, that is nearly eight times higher than that of the fragment calculation. Even though the fragmentation scheme is extremely simple, the resulting error is only 0.6mE_h, compared to the canonical calculation. A profiling analysis of the runtime revealed that $\approx 90\%$ of the spent time is due to the wave function calculations and analyses in Psi4 and GDMA while the remaining 10% mainly comprise file handling and parsing in Spicy. Construction costs of neighbor lists, groups as well as fragments are negligible ($\leq 2\%$).

In addition to these calculations, *Spicy* includes many additional test cases. Interested readers are referred to *Spicy's* online presence under https://gitlab.com/theoretical-chemistry-jena/quantum-chemistry/Spicy.
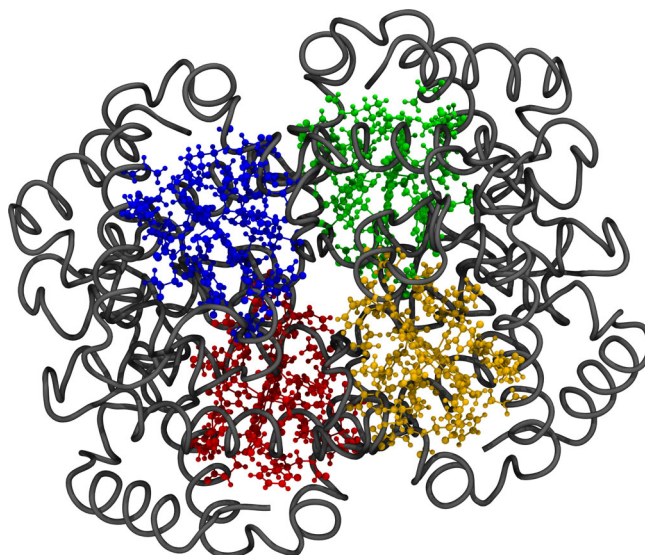
FIGURE 10 Visualization of the MC partitioning of hemoglobin. Each group of colored atoms represents a distinct sublayer of the real system.
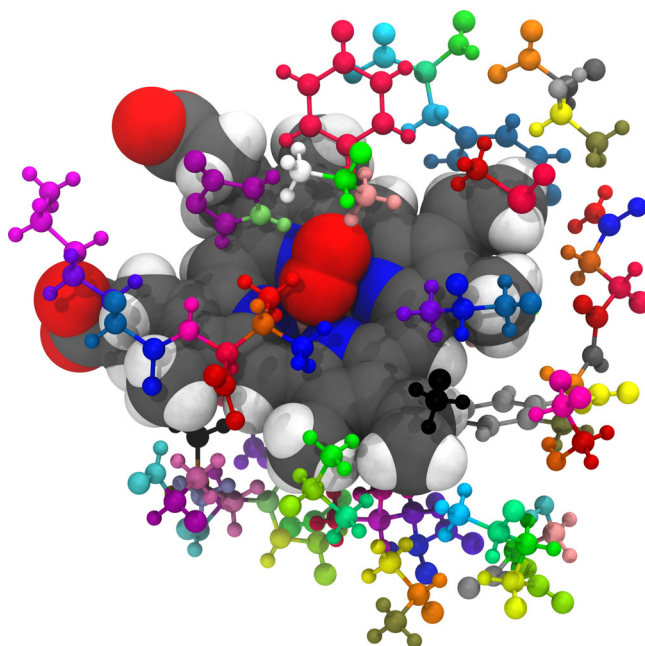
FIGURE 11 Close-up on one of the model layers depicted in Figure 10. The van der Waals spheres represent the atoms of the home unit in the innermost layer. The ball and stick model represents atoms belonging to the intermediate layer, with each color denoting a different group. In the intermediate layer fragment methods are applied and the color coded groups from fragments via overlapping ego-graphs of length 3 (see Section 2.3). Multipoles obtained in fragment calculations of the intermediate layers are used to polarize the wavefunction in the innermost layers (see also Figure 12).

4.2 | Application to hemoglobin

As a demonstration of *Spicy's* extended capabilities and flexibility, this section presents an application of a complex ONIOM setup for the oxy-hemoglobin macromolecule (PDB code 6BB5[121]). As a protein with multiple active sites, it is a typical use case for MC-ONIOM*n*.
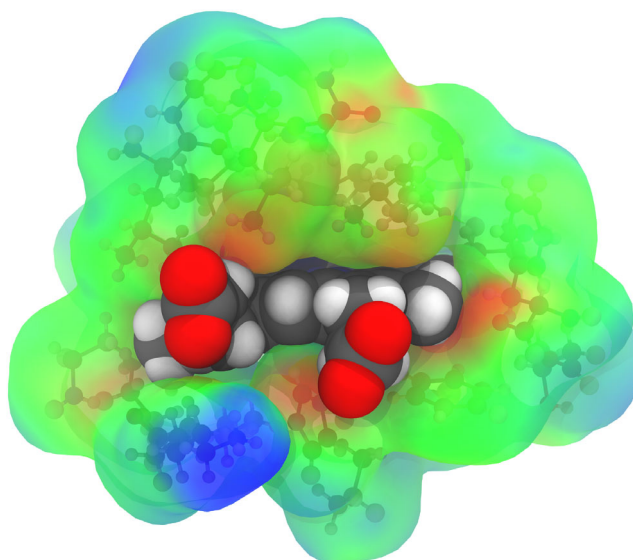
FIGURE 12 One home unit of hemoglobin embedded in the polarizing field of the surrounding protein fragments. Multipoles were obtained at the cost-efficient GFN-2 level to enhance the accuracy of the Hartree–Fock description of the inner heme electronic structure. Blue color on the isosurface denotes positive electrostatic potential while a red tint signifies negative electrostatic potential.

A partitioning for an ONIOM calculation of hemoglobin arises naturally. The real, outermost layer includes all atoms and must be treated with an efficient method; xTB's GFN-FF[106] is a sensible choice. Dividing according to the individual heme units leads to a MC-ONIOM setup (see Figure 10). All groups (as detected by SMF) within 0.5 nm of each metal center are collected into "pockets," forming four centers. These layers are treated with the GMBE formalism using GFN-2.[118] Figure 11 depicts one such pocket. Note that the automatically detected groups are quite small, rarely exceeding the size of a benzene ring. Finally, in each of these pockets, the actual heme units form the deepest sublayers. For these, Turbomole's implementation of HF-3c[122] provides the electronic structure. The converged wavefunctions of the heme centers were checked by SCF stability analyses.

Figure 12 demonstrates the embedding of the inner heme layer in the electrostatic field. The inclusion of the electrostatic field induces an energetic shift of $0.16E_h$, or more than 4 eV, in the energy of the heme unit. All of these electrostatic interactions would have been lost completely in a simple mechanical embedding scheme.

This calculation of a macromolecule with over 9000 atoms could be conducted on a local workstation in a short period of time ($\approx 20\,\text{min}$ with the GFN-FF topology pre-generated, running on a Intel Xeon W-2155 CPU) while still delivering high quality electronic structure at the important reactive sites.

5 | OUTLOOK AND CONCLUSIONS

In this contribution, we have presented the *Spicy* program, a comprehensive free implementation of ONIOM and fragment methods. Importantly Spicy offers a combination of unique features.

- Spicy's ONIOM implementation allows setups with any number of layers.
- MC-ONIOM methods allow a tree-like structure of the multilayer setup with an arbitrary number of centers per layer to reduce computational costs for weakly interacting centers.
- A multipolar electronic embedding scheme provides higher accuracy for electrostatic interactions.
- Support for complex layer definitions via an easy-to-use domain-specific language.
- A set of generation algorithms and implementation of FCRs allows utilization of a wide range of fragment methods.
- Fragment methods, the MC-ONIOM method and electronic embedding can be combined flexibly to obtain generalized or extended ONIOM-like methods.
- A micro-cycle driven optimization scheme provides efficient structure optimizations on large systems with different coordinate systems and optimizers.

- Utilizing a wrapper approach, more computational methods than available in a single program can be combined.

This previously unavailable flexibility in the system setup in combination with the large range of available methods in the underlying computational chemistry programs, enables calculations on systems, that would otherwise be inaccessible, as for example, force-field parameters may be missing.

Spicy relies on external, well-tested, and performant codes whenever possible, an approach that has gained traction in recent years and enables more rapid development, specialization, and tuning of individual components.[107,109,123–125] With Psi4 and Turbomole, two performant quantum chemistry codes with extended capabilities for wavefunction and density functional theory (DFT) calculations are interfaced. xTB provides access to fast, semiempirical methods, applicable to a wide range of systems. By interfacing pysisyphus, a powerful optimization engine is available, and the GDMA program provides facilities for wavefunction analysis.

We have demonstrated *Spicy's* ability to produce correct results for MC-ONIOMn calculations, micro-cycle driven optimizations, and fragment calculations. To the best of our knowledge, the MC partitioning enabled the first calculation on the notoriously difficult hemoglobin, where all four heme centers were calculated using quantum-mechanical methods. GMBE was used to obtain high-level multipoles in the pockets surrounding the hemes and finally wavefunction calculations treated each heme separately in the electric field of the protein backbone, expanded up to quadrupoles.

Among other applications, *Spicy* will facilitate the computational investigations of photocatalysts in semiconducting polymers as well as self-healing polymers in our group.

While *Spicy* is a young program in its early stages of development, it already implements an extensive set of methods. Near future development efforts will concentrate on further generalization of fragment and ONIOM methods and implement a multilayer-FCR scheme[62] as a superset of the presented ONIOM and fragment schemes. The implementation of a network-distributed scheduling system will facilitate massively parallel fragment calculations, while at the same time, we aim to further reduce resource consumption by means of sparse linear algebra and streaming optimizations. Mid-term the development will focus on molecular dynamics and dynamic system partitioning in the spirit of ONIOM-XS.[64] In a long-term perspective we aim to provide multilayer excited state calculations in *Spicy*, that is, by explicitly accounting for embedding of excited states.

Spicy is built as a platform open to contributions, and we hope to provide a useful tool and basis for further application and developments in fragment- and ONIOM-like multiscale methods.

AUTHOR CONTRIBUTIONS

Phillip Seeber: Conceptualization (lead); data curation (equal); formal analysis (lead); investigation (lead); methodology (lead); project administration (supporting); software (lead); validation (equal); visualization (lead); writing – original draft (lead); writing – review and editing (supporting). **Sebastian Seidenath:** Conceptualization (supporting); data curation (equal); formal analysis (supporting); investigation (supporting); methodology (supporting); software (supporting); validation (equal); visualization (equal); writing – original draft (supporting). **Johannes Steinmetzer:** Investigation (supporting); methodology (supporting); software (supporting); validation (supporting); writing – review and editing (equal). **Stefanie Gräfe:** Conceptualization (supporting); funding acquisition (lead); project administration (lead); resources (lead); supervision (lead); writing – review and editing (equal).

ACKNOWLEDGMENTS

FUNDING INFORMATION

CONFLICT OF INTEREST

The authors have no conflict of interest.

DATA AVAILABILITY STATEMENT

The data that support the findings of this study are openly available in Spicy's GitLab repository at https://gitlab.com/theoretical-chemistry-jena/quantum-chemistry/Spicy.

ORCID

Phillip Seeber https://orcid.org/0000-0002-4968-7726
Sebastian Seidenath https://orcid.org/0000-0001-9075-9819
Johannes Steinmetzer https://orcid.org/0000-0003-2493-6893
Stefanie Gräfe https://orcid.org/0000-0002-1747-5809

RELATED WIREs ARTICLES

Turbomole
Psi4: An open-source ab initio electronic structure program

ENDNOTE

* Metals = {Li...Al, K...Ga, Rb...Sn, Cs...Bi, Fr...Og}

REFERENCES

1. Dykstra C, Frenking G, Kim K, Scuseria G. Theory and applications of computational chemistry: the first forty years. Amsterdam: Elsevier; 2011.
2. Zheng J, Wang D, Thiel W, Shaik S. QM/MM study of mechanisms for compound I formation in the catalytic cycle of cytochrome P450cam. J Am Chem Soc. 2006;128:13204–15. https://doi.org/10.1021/ja063439l
3. Mebs S, Kositzki R, Duan J, Kertess L, Senger M, Wittkamp F, et al. Hydrogen and oxygen trapping at the H-cluster of [FeFe]-hydrogenase revealed by site-selective spectroscopy and QM/MM calculations. Biochim Biophys Acta (BBA) - Bioenerg. 2018;1859(1): 28–41. https://doi.org/10.1016/j.bbabio.2017.09.003
4. Nastase SAF, Logsdail AJ, Catlow CRA. QM/MM study of the reactivity of zeolite bound methoxy and carbene groups. Phys Chem Chem Phys. 2021;23(32):17634–44. https://doi.org/10.1039/d1cp02535j
5. Frate GD, Bellina F, Mancini G, Marianetti G, Minei P, Pucci A, et al. Tuning of dye optical properties by environmental effects: a QM/MM and experimental study. Phys Chem Chem Phys. 2016;18(14):9724–33. https://doi.org/10.1039/c6cp00841k
6. Khaliullin RZ, VandeVondele J, Hutter J. Efficient linear-scaling density functional theory for molecular systems. J Chem Theory Comput. 2013;9:4421–7. https://doi.org/10.1021/ct400595k
7. Mountjoy J, Todd M, Mosey NJ. Exact exchange with non-orthogonal generalized Wannier functions. J Chem Phys. 2017;146(10): 104108. https://doi.org/10.1063/1.4977783
8. Prentice JCA, Aarons J, Womack JC, Allen AEA, Andrinopoulos L, Anton L, et al. The ONETEP linear-scaling density functional theory program. J Chem Phys. 2020;152(17):174111. https://doi.org/10.1063/5.0004445
9. VandeVondele J, Borštnik U, Hutter J. Linear scaling self-consistent field calculations with millions of atoms in the condensed phase. J Chem Theory Comput. 2012;8:3565–73. https://doi.org/10.1021/ct200897x
10. Niklasson AMN, Tymczak CJ, Challacombe M. Trace resetting density matrix purification in O(N) selfconsistent-field theory. J Chem Phys. 2003;118(19):8611–20. https://doi.org/10.1063/1.1559913
11. Shao Y, Saravanan C, Head-Gordon M, White CA. Curvy steps for density matrix-based energy minimization: application to large-scale self-consistent-field calculations. J Chem Phys. 2003;118(14):6144–51. https://doi.org/10.1063/1.1558476
12. Guo Y, Riplinger C, Becker U, Liakos DG, Minenkov Y, Cavallo L, et al. Communication: an improved linear scaling perturbative triples correction for the domain based local pair-natural orbital based singles and doubles coupled cluster method [DLPNO-CCSD(T)]. J Chem Phys. 2018;148(1):011101. https://doi.org/10.1063/1.5011798
13. Guo Y, Becker U, Neese F. Comparison and combination of "direct" and fragment based local correlation methods: cluster in molecules and domain based local pair natural orbital perturbation and coupled cluster theories. J Chem Phys. 2018;148(12):124117. https://doi.org/10.1063/1.5021898
14. Saitow M, Becker U, Riplinger C, Valeev EF, Neese F. A new near-linear scaling, efficient and accurate, open-shell domain-based local pair natural orbital coupled cluster singles and doubles theory. J Chem Phys. 2017;146(16):164105. https://doi.org/10.1063/1.4981521
15. Ma Q, Werner HJ. Explicitly correlated local coupled-cluster methods using pair natural orbitals. Wiley Interdiscip Rev Comput Mol Sci. 2018;8:e1371. https://doi.org/10.1002/wcms.1371
16. Nagy PR, Samu G, Kállay M. An integral-direct linear-scaling second-order Møller–Plesset approach. J Chem Theory Comput. 2016; 12(10):4897–914. https://doi.org/10.1021/acs.jctc.6b00732
17. Nagy PR, Kállay M. Optimization of the linear-scaling local natural orbital CCSD(T) method: redundancy-free triples correction using Laplace transform. J Chem Phys. 2017;146(21):214106. https://doi.org/10.1063/1.4984322

18. Nagy PR, Samu G, Kállay M. Optimization of the linear-scaling local natural orbital CCSD(T) method: improved algorithm and benchmark applications. J Chem Theory Comput. 2018;14(8):4193–215. https://doi.org/10.1021/acs.jctc.8b00442

19. Nagy PR, Kállay M. Approaching the basis set limit of CCSD(T) energies for large molecules with local natural orbital coupled-cluster methods. J Chem Theory Comput. 2019;15(10):5275–98. https://doi.org/10.1021/acs.jctc.9b00511

20. Hégely B, Nagy PR, Ferenczy GG, Kállay M. Exact density functional and wave function embedding schemes based on orbital localization. J Chem Phys. 2016;145(6):064107. https://doi.org/10.1063/1.4960177

21. Knizia G, Chan GKL. Density matrix embedding: a strong-coupling quantum embedding theory. J Chem Theory Comput. 2013;9(3):1428–32. https://doi.org/10.1021/ct301044e

22. Durrant JD, Kochanek SE, Casalino L, Ieong PU, Dommer AC, Amaro RE. Mesoscale all-atom influenza virus simulations suggest new substrate binding mechanism. ACS Cent Sci. 2020;6(2):189–96. https://doi.org/10.1021/acscentsci.9b01071

23. Gao P, Duan X, Zhang T, Zhang M, Schmidt B, Zhang X, et al. Millimeter-scale and billion-atom reactive force field simulation on sunway taihulight. IEEE Trans Parallel Distrib Syst. 2020;31(12):2954–67. https://doi.org/10.1109/tpds.2020.3008499

24. Warshel A, Karplus M. Calculation of ground and excited state potential surfaces of conjugated molecules. I. Formulation and parametrization. J Am Chem Soc. 1972;94(16):5612–25. https://doi.org/10.1021/ja00771a014

25. Warshel A, Levitt M. Theoretical studies of enzymic reactions: dielectric, electrostatic and steric stabilization of the carbonium ion in the reaction of lysozyme. J Mol Biol. 1976;103(2):227–49. https://doi.org/10.1016/0022-2836(76)90311-9

26. Magalhães RP, Fernandes HS, Sousa SF. Modelling enzymatic mechanisms with QM/MM approaches: current status and future challenges. Isr J Chem. 2020;60(7):655–66. https://doi.org/10.1002/ijch.202000014

27. Ahmadi S, Barrios Herrera L, Chehelamirani M, Hostaš J, Jalife S, Salahub DR. Multiscale modeling of enzymes: QM-cluster, QM/MM, and QM/MM/MD: a tutorial review. Int J Quant Chem. 2018;118(9):e25558. https://doi.org/10.1002/qua.25558

28. Svensson M, Humbel S, Morokuma K. Energetics using the single point IMOMO (integrated molecular orbital+molecular orbital) calculations: choices of computational levels and model system. J Chem Phys. 1996;105(9):3654–61. https://doi.org/10.1063/1.472235

29. Vreven T, Byun KS, Komáromi I, Dapprich S, Montgomery JA Jr, Morokuma K, et al. Combining quantum mechanics methods with molecular mechanics methods in ONIOM. J Chem Theory Comput. 2006;2(3):815–26. https://doi.org/10.1021/ct050289g

30. Chung LW, Sameera WMC, Ramozzi R, Page AJ, Hatanaka M, Petrova GP, et al. The ONIOM method and its applications. Chem Rev. 2015;115(12):5678–796. https://doi.org/10.1021/cr5004419

31. Bondanza M, Jacquemin D, Mennucci B. Excited states of xanthophylls revisited: toward the simulation of biologically relevant systems. J Phys Chem Lett. 2021;12(28):6604–12. https://doi.org/10.1021/acs.jpclett.1c01929

32. Lapillo M, Cignoni E, Cupellini L, Mennucci B. The energy transfer model of nonphotochemical quenching: lessons from the minor CP29 antenna complex of plants. Biochim Biophys Acta (BBA) – Bioenerg. 2020;1861(11):148282. https://doi.org/10.1016/j.bbabio.2020.148282

33. Rosnik AM, Curutchet C. Theoretical characterization of the spectral density of the water-soluble chlorophyll-binding protein from combined quantum mechanics/molecular mechanics molecular dynamics simulations. J Chem Theory Comput. 2015;11(12):5826–37. https://doi.org/10.1021/acs.jctc.5b00891

34. Menger MFSJ, Caprasecca S, Mennucci B. Excited-state gradients in polarizable QM/MM models: an induced dipole formulation. J Chem Theory Comput. 2017;13(8):3778–86. https://doi.org/10.1021/acs.jctc.7b00475

35. Kupfer S, Zedler L, Guthmuller J, Bode S, Hager MD, Schubert US, Popp J, Gräfe S, Dietzek B Self-healing mechanism of metallopolymers investigated by QM/MM simulations and Raman spectroscopy Phys Chem Chem Phys 2014;16:12422–12432. doi: https://doi.org/10.1039/c4cp00562g.

36. Eichler U, Kölmel CM, Sauer J. Combining ab initio techniques with analytical potential functions for structure predictions of large systems: method and application to crystalline silica polymorphs. J Comput Chem. 1997;18:463–77.

37. Sierka M, Sauer J. Finding transition structures in extended systems: a strategy based on a combined quantum mechanics–empirical valence bond approach. J Chem Phys. 2000;112(16):6983–96. https://doi.org/10.1063/1.481296

38. Amthor S, Hernández-Castillo D, Maryasin B, Seeber P, Mengele AK, Gräfe S, et al. Strong ligand stabilization based on-extension in a series of ruthenium terpyridine water oxidation catalysts. Chem Eur J. 2021;27(68):16871–8. https://doi.org/10.1002/chem.202102905

39. Golze D, Iannuzzi M, Nguyen MT, Passerone D, Hutter J. Simulation of adsorption processes at metallic interfaces: an image charge augmented QM/MM approach. J Chem Theory Comput. 2013;9(11):5086–97. https://doi.org/10.1021/ct400698y

40. Doitomi K, Xu K, Hirao H. The mechanism of an asymmetric ring-opening reaction of epoxide with amine catalyzed by a metal–organic framework: insights from combined quantum mechanics and molecular mechanics calculations. Dalton Trans. 2017;46(11):3470–81. https://doi.org/10.1039/c6dt04745a

41. Walsh A, Buckeridge J, Catlow CRA, Jackson AJ, Keal TW, Miskufova M, et al. Limits to doping of wide band gap semiconductors. Chem Mater. 2013;25(15):2924–6. https://doi.org/10.1021/cm402237s

42. Taştan Ü, Seeber P, Kupfer S, Ziegenbalg D. Photochlorination of toluene – the thin line between intensification and selectivity. Part 2: selectivity. React Chem Eng. 2021;6(1):90–9. https://doi.org/10.1039/d0re00366b

43. Kratz EG, Walker AR, Lagardère L, Lipparini F, Piquemal JP, Andrés CG. LICHEM: a QM/MM program for simulations with multipolar and polarizable force fields. J Comput Chem. 2016;37(11):1019–29. https://doi.org/10.1002/jcc.24295

44. Thompson MA. QM/MMpol: a consistent model for solute/solvent polarization. Application to the aqueous solvation and spectroscopy of formaldehyde, acetaldehyde, and acetone. J Phys Chem. 1996;100(34):14492–507. https://doi.org/10.1021/jp960690m

45. Lu Y, Farrow MR, Fayon P, Logsdail AJ, Sokol AA, Catlow CRA, et al. Open-source, python-based redevelopment of the chemshell multiscale QM/MM environment. J Chem Theory Comput. 2018;15(2):1317–28. https://doi.org/10.1021/acs.jctc.8b01036

46. Larsen AH, Jørgen Mortensen J, Blomqvist J, Castelli IE, Christensen R, Dułak M, et al. The atomic simulation environment—a python library for working with atoms. J Phys Condens Matter. 2017;29(27):273002.

47. Řezáč J. Cuby: an integrative framework for computational chemistry. J Comput Chem. 2016;37(13):1230–7. https://doi.org/10.1002/jcc.24312

48. Neese F. The ORCA program system. WIREs Comput Mol Sci. 2012;2(1):73–8. https://doi.org/10.1002/wcms.81

49. Neese F. Software update: the ORCA program system, version 4.0. WIREs Comput Mol Sci. 2018;8(1):e1327. https://doi.org/10.1002/wcms.1327

50. Bjornsson R, Bühl M. Modeling molecular crystals by QM/MM: self-consistent electrostatic embedding for geometry optimizations and molecular property calculations in the solid. J Chem Theory Comput. 2012;8(2):498–508. https://doi.org/10.1021/ct200824r

51. Dittmer A, Izsák R, Neese F, Maganas D. Accurate band gap predictions of semiconductors in the framework of the similarity transformed equation of motion coupled cluster theory. Inorg Chem. 2019;58(14):9303–15. https://doi.org/10.1021/acs.inorgchem.9b00994

52. Kállay M, Nagy PR, Mester D, Rolik Z, Samu G, Csontos J, et al. The MRCC program system: accurate quantum chemistry from water to proteins. J Chem Phys. 2020;152(7):074107. https://doi.org/10.1063/1.5142048

53. Vreven T, Mennucci B, da Silva CO, Morokuma K, Tomasi J. The ONIOM-PCM method: combining the hybrid molecular orbital method and the polarizable continuum model for solvation. Application to the geometry and properties of a merocyanine in solution. J Chem Phys. 2001;115(1):62–72. https://doi.org/10.1063/1.1376127

54. Frisch MJ, Trucks GW, Schlegel HB, Scuseria GE, Robb MA, Cheeseman JR, et al. Gaussian-16 Revision C.01. Wallingford, CT: Gaussian Inc.; 2016.

55. Chettri A et al. A molecular photosensitizer in a porous block copolymer matrix-implications for the design of photocatalytically active membranes. Chem Eur J. 2021;27(68):17049–58. https://doi.org/10.1002/chem.202102377

56. Feng K, Peng ML, Wang DH, Zhang LP, Tung CH, Wu LZ. Silica- and polymer-supported platinum(II) polypyridyl complexes: synthesis and application in photosensitized oxidation of alkenes. Dalton Trans. 2009;44:9794–9. https://doi.org/10.1039/b916488j

57. Whitford D. Proteins: structure and function. New York Wiley; 2005.

58. Perutz MF, Rossmann MG, Cullis AF, Muirhead H, Will G, North ACT. Structure of haemoglobin: a three-dimensional Fourier synthesis at 5.5-A resolution, obtained by X-ray analysis. Nature. 1960;185(4711):416–22. https://doi.org/10.1038/185416a0

59. Hopkins BW, Tschumper GS. A multicentered approach to integrated QM/QM calculations. Applications to multiply hydrogen bonded systems. J Comput Chem. 2003;24(13):1563–8. https://doi.org/10.1002/jcc.10319

60. Chung LW, Hirao H, Li X, Morokuma K. The ONIOM method: its foundation and applications to metalloenzymes and photobiology. Wiley Interdiscip Rev Comput Mol Sci. 2012;2(2):327–50. https://doi.org/10.1002/wcms.85

61. Richard RM, Herbert JM. A generalized many-body expansion and a unified view of fragment-based methods in electronic structure theory. J Chem Phys. 2012;137(6):064113. https://doi.org/10.1063/1.4742816

62. Hellmers J, König C. A unified and flexible formulation of molecular fragmentation schemes. J Chem Phys. 2021;155(16):164105. https://doi.org/10.1063/5.0059598

63. Xie W, Song L, Truhlar DG, Gao J. The variational explicit polarization potential and analytical first derivative of energy: towards a next generation force field. J Chem Phys. 2008;128(23):234108. https://doi.org/10.1063/1.2936122

64. Kerdcharoen T, Morokuma K. ONIOM-XS: an extension of the ONIOM method for molecular simulation in condensed phase. Chem Phys Lett. 2002;355(3-4):257–62. https://doi.org/10.1016/s0009-2614(02)00210-5

65. Stone A. Distributed multipole analysis, or how to describe a molecular charge distribution. Chem Phys Lett. 1981;83(2):233–9. https://doi.org/10.1016/0009-2614(81)85452-8

66. Stone AJ. Distributed multipole analysis: stability for large basis sets. J Chem Theory Comput. 2005;1(6):1128–32. https://doi.org/10.1021/ct050190+

67. Stone A. The theory of intermolecular forces. 2nd ed. New York Oxford University Press; 2013. https://doi.org/10.1093/acprof:oso/9780199672394.001.0001

68. Steinmetzer J, Kupfer S, Gräfe S. Pysisyphus: exploring potential energy surfaces in ground and excited states. Int J Quant Chem. 2021;121(3):e26390. https://doi.org/10.1002/qua.26390

69. Maseras F, Morokuma K. IMOMM: a new integratedab initio + molecular mechanics geometry optimization scheme of equilibrium structures and transition states. J Comput Chem. 1995;16(9):1170–9. https://doi.org/10.1002/jcc.540160911

70. Zhang Y, Lee T, Yang W. A pseudobond approach to combining quantum mechanical and molecular mechanical methods. J Chem Phys. 1999;110(1):46–54. https://doi.org/10.1063/1.478083

71. DiLabio GA, Hurley MM, Christiansen PA. Simple one-electron quantum capping potentials for use in hybrid QM/MM studies of biological molecules. J Chem Phys. 2002;116:9578–84.

72. Gamoke BC, Das U, Hratchian HP, Raghavachari K. Divalent pseudoatoms for modeling Si(100) surfaces. J Chem Phys. 2013;139(16):164708. https://doi.org/10.1063/1.4825402

73. Philipp DM, Friesner RA. Mixedab initio QM/MM modeling using frozen orbitals and tests with alanine dipeptide and tetrapeptide. J Comput Chem. 1999;20:1468–94.

74. Gao J, Amara P, Alhambra C, Field MJ. A generalized hybrid orbital (GHO) method for the treatment of boundary atoms in combined QM/MM calculations. Chem A Eur J. 1998;102(24):4714–21. https://doi.org/10.1021/jp9809890

75. Théry V, Rinaldi D, Rivail JL, Maigret B, Ferenczy GG. Quantum mechanical computations on very large molecular systems: the local self-consistent field method. J Comput Chem. 1994;15(3):269–82. https://doi.org/10.1002/jcc.540150303

76. Field MJ, Bash PA, Karplus M. A combined quantum mechanical and molecular mechanical potential for molecular dynamics simulations. J Comput Chem. 1990;11(6):700–33. https://doi.org/10.1002/jcc.540110605

77. Singh UC, Kollman PA. A combinedab initio quantum mechanical and molecular mechanical method for carrying out simulations on complex molecular systems: applications to the CH3Cl + Cl? Exchange reaction and gas phase protonation of polyethers. J Comput Chem. 1986;7(6):718–30. https://doi.org/10.1002/jcc.540070604

78. Dapprich S, Komáromi I, Byun K, Morokuma K, Frisch MJ. A new ONIOM implementation in Gaussian98. Part I. the calculation of energies, gradients, vibrational frequencies and electric field derivatives. J Mol Struct (Theochem). 1999;461-462:1–21. https://doi.org/10.1016/S0166-1280(98)00475-8

79. Mulliken RS. Electronic population analysis on LCAO–MO molecular wave functions. I. J Chem Phys. 1955;23(10):1833–40. https://doi.org/10.1063/1.1740588

80. Löwdin PO. On the non-orthogonality problem connected with the use of atomic wave functions in the theory of molecules and crystals. J Chem Phys. 1950;18(3):365–75. https://doi.org/10.1063/1.1747632

81. Breneman CM, Wiberg KB. Determining atom-centered monopoles from molecular electrostatic potentials. The need for high sampling density in formamide conformational analysis. J Comput Chem. 1990;11(3):361–73. https://doi.org/10.1002/jcc.540110311

82. Marefat Khah A, Reinholdt P, Olsen JMH, Kongsted J, Hättig C. Avoiding electron spill-out in QM/MM calculations on excited states with simple pseudopotentials. J Chem Theory Comput. 2020;16(3):1373–81. https://doi.org/10.1021/acs.jctc.9b01162

83. Mayhall NJ, Raghavachari K, Hratchian HP. ONIOM-based QM:QM electronic embedding method using Löwdin atomic charges: energies and analytic gradients. J Chem Phys. 2010;132(11):114107. https://doi.org/10.1063/1.3315417

84. Hopkins BW, Tschumper GS. Multicentred QM/QM methods for overlapping model systems. Mol Phys. 2005;103(2-3):309–15. https://doi.org/10.1080/00268970512331317291

85. Hratchian HP, Parandekar PV, Raghavachari K, Frisch MJ, Vreven T. QM:QM electronic embedding using Mulliken atomic charges: energies and analytic gradients in an ONIOM framework. J Chem Phys. 2008;128(3):034107. https://doi.org/10.1063/1.2814164

86. Rivera M, Dommett M, Crespo-Otero R. ONIOM(QM:QM) electrostatic embedding schemes for photochemistry in molecular crystals. J Chem Theory Comput. 2019;15(4):2504–16. https://doi.org/10.1021/acs.jctc.8b01180

87. Gao Q, Yokojima S, Fedorov DG, Kitaura K, Sakurai M, Nakamura S. Octahedral point-charge model and its application to fragment molecular orbital calculations of chemical shifts. Chem Phys Lett. 2014;593:165–73. https://doi.org/10.1016/j.cplett.2014.01.001

88. Devereux M, Raghunathan S, Fedorov DG, Meuwly M. A novel, computationally efficient multipolar model employing distributed charges for molecular dynamics simulations. J Chem Theory Comput. 2014;10(10):4229–41. https://doi.org/10.1021/ct500511t

89. Ponder JW, Wu C, Ren P, Pande VS, Chodera JD, Schnieders MJ, et al. Current status of the AMOEBA polarizable force field. J Phys Chem B. 2010;114(8):2549–64. https://doi.org/10.1021/jp910674d

90. Dahlke EE, Truhlar DG. Electrostatically embedded many-body expansion for large systems, with applications to water clusters. J Chem Theory Comput. 2007;3(1):46–53. https://doi.org/10.1021/ct600253j

91. Deev V, Collins MA. Approximateab initioenergies by systematic molecular fragmentation. J Chem Phys. 2005;122(15):154102. https://doi.org/10.1063/1.1879792

92. Collins MA, Cvitkovic MW, Bettens RPA. The combined fragmentation and systematic molecular fragmentation methods. Acc Chem Res. 2014;47(9):2776–85. https://doi.org/10.1021/ar500088d

93. Zhang DW, Zhang JZH. Molecular fractionation with conjugate caps for full quantum mechanical calculation of protein–molecule interaction energy. J Chem Phys. 2003;119(7):3599–605. https://doi.org/10.1063/1.1591727

94. Hestenes M, Stiefel E. Methods of conjugate gradients for solving linear systems. J Res Natl Bur Stand. 1952;49(6):409. https://doi.org/10.6028/jres.049.044

95. Liu DC, Nocedal J. On the limited memory BFGS method for large scale optimization. Math Program. 1989;45(1-3):503–28. https://doi.org/10.1007/bf01589116

96. Wang LP, Song C. Geometry optimization made simple with translation and rotation coordinates. J Chem Phys. 2016;144(21):214108.

97. Kästner J, Thiel S, Senn HM, Sherwood P, Thiel W. Exploiting QM/MM capabilities in geometry optimization: a microiterative approach using electrostatic embedding. J Chem Theory Comput. 2007;3(3):1064–72. https://doi.org/10.1021/ct600346p

98. Vreven T, Morokuma K, Farkas Ö, Schlegel HB, Frisch MJ. Geometry optimization with QM/MM, ONIOM, and other combined methods. I. Microiterations and constraints. J Comput Chem. 2003;24(6):760–9. https://doi.org/10.1002/jcc.10156

99. Billeter SR, Turner AJ, Thiel W. Linear scaling geometry optimisation and transition state search in hybrid delocalised internal coordinates. Phys Chem Chem Phys. 2000;2(10):2177–86. https://doi.org/10.1039/a909486e

100. Bakowies D, Thiel W. Hybrid models for combined quantum mechanical and molecular mechanical approaches. J Phys Chem. 1996;100(25):10580–94. https://doi.org/10.1021/jp9536514

101. Harris T, Marlow S, Peyton-Jones S and Herlihy M. Composable memory transactions. In: Proceedings of the Tenth ACM SIGPLAN Symposium on Principles and Practice of Parallel Programming. PPoPP05. Chicago: Association for Computing Machinery; 2005. p. 48–60. https://doi.org/10.1145/1065944.1065952.

102. Kuleshevich A. Massiv: Efficient Haskell Arrays featuring Parallel computation. https://github.com/lehins/massiv

103. Okasaki C, Gill A. Fast mergeable integer maps. In: Workshop on ML; 1998. p. 77–86.

104. Morrison DR. PATRICIA—practical algorithm to retrieve information coded in alphanumeric. J ACM. 1968;15(4):514–34. https://doi.org/10.1145/321479.321481

105. Humphrey W, Dalke A, Schulten K. VMD – visual molecular dynamics. J Mol Graph. 1996;14:33–8.

106. Bannwarth C, Caldeweyher E, Ehlert S, Hansen A, Pracht P, Seibert J, et al. Extended tight-binding quantum chemistry methods. WIREs Comput Mol Sci. 2021;11(2):e1493. https://doi.org/10.1002/wcms.1493

107. Smith DGA, Burns LA, Simmonett AC, Parrish RM, Schieber MC, Galvelis R, et al. PSI4 1.4: open-source software for high-throughput quantum chemistry. J Chem Phys. 2020;152(18):184108. https://doi.org/10.1063/5.0006002

108. Balasubramani SG, Chen GP, Coriani S, Diedenhofen M, Frank MS, Franzke YJ, et al. TURBOMOLE: modular program suite for *ab initio* quantum-chemical and condensedmatter simulations. J Chem Phys. 2020;152(18):184107. https://doi.org/10.1063/5.0004635

109. Smith DGA, Lolinco AT, Glick ZL, Lee J, Alenaizan A, Barnes TA, et al. Quantum chemistry common driver and databases (QCDB) and quantum chemistry engine (QCEngine): automation and interoperability among computational chemistry programs. J Chem Phys. 2021;155(20):204801. https://doi.org/10.1063/5.0059356

110. Kapil V, Rossi M, Marsalek O, Petraglia R, Litman Y, Spura T, et al. i-PI 2.0: a universal force engine for advanced molecular simulations. Comput Phys Commun. 2019;236:214–23. https://doi.org/10.1016/j.cpc.2018.09.020

111. Marlow S. Haskell 2010 language report.

112. Nix Manual. https://nixos.org/manual/nix/stable/

113. Nixpkgs Manual. https://nixos.org/manual/nixpkgs/stable/

114. https://github.com/markuskowa/NixOS-QChem

115. Kowalewski M, Seeber P. Sustainable packaging of quantum chemistry software with the nix package manager. Int J Quant Chem. 2022;122(9):e26872. https://doi.org/10.1002/qua.26872

116. Becke AD. Density-functional thermochemistry. III. The role of exact exchange. J Chem Phys. 1993;98(7):5648–52. https://doi.org/10.1063/1.464913

117. Dunning TH. Gaussian basis sets for use in correlated molecular calculations. I. The atoms boron through neon and hydrogen. J Chem Phys. 1989;90(2):1007–23. https://doi.org/10.1063/1.456153

118. Bannwarth C, Ehlert S, Grimme S. GFN2-xTB—an accurate and broadly parametrized self-consistent tight-binding quantum chemical method with multipole electrostatics and density-dependent dispersion contributions. J Chem Theory Comput. 2019;15(3):1652–71. https://doi.org/10.1021/acs.jctc.8b01176

119. Møller C, Plesset MS. Note on an approximation treatment for many-electron systems. Phys Rev. 1934;46:618–22. https://doi.org/10.1103/PhysRev.46.618

120. Weigend F, Ahlrichs R. Balanced basis sets of split valence, triple zeta valence and quadruple zeta valence quality for H to Rn: design and assessment of accuracy. Phys Chem Chem Phys. 2005;7(18):3297–305. https://doi.org/10.1039/B508541A

121. Gumpper R, Terrell J, Luo M. Human oxy-hemoglobin. PDB. 2018. https://doi.org/10.2210/pdb6bb5/pdb

122. Grimme S, Brandenburg JG, Bannwarth C, Hansen A. Consistent structures and interactions by density functional theory with small atomic orbital basis sets. J Chem Phys. 2015;143(5):054107. https://doi.org/10.1063/1.4927476

123. Gezelter JD. Open source and open data should Be standard practices. J Phys Chem Lett. 2015;6(7):1168–9. https://doi.org/10.1021/acs.jpclett.5b00285

124. Jacob CR. How open is commercial scientific software? J Phys Chem Lett. 2016;7(2):351–3. https://doi.org/10.1021/acs.jpclett.5b02609

125. https://danielskatzblog.wordpress.com/2015/08/27/the-price-of-open-source-software-a-joint-response/